Computational Mechanics
https://doi.org/10.1007/s00466-025-02616-2

ORIGINAL PAPER

A nonlinear 4-node shell element with one point quadrature and stabilization based on a Hu–Washizu variational formulation

Friedrich Gruttmann[1] · **Werner Wagner**[2]

Received: 9 January 2025 / Accepted: 22 February 2025

Abstract
In this paper a robust and effective 4–node shell element for the structural analysis of thin structures is described. A Hu–Washizu functional with independent displacements, stress resultants and shell strains is the variational basis of the formulation. With application of three basic assumptions within the FE formulation a stabilized one point integrated element comes out automatically. Besides static computations it can be used for dynamic problems with explicit or implicit time integration without further adaptions. The element possesses the correct rank and fulfills the membrane and bending patch test. The stabilization terms can be integrated analytically and do not require an input of problem dependent control parameters. In contrast to several approaches the results are not path dependent for hyperelastic material behavior. This unphysical behavior follows when the material matrix of the last load increment is used in the stabilization matrix to preserve quadratic convergence in the Newton-Raphson iteration. The element possesses the well-known robustness of Hu–Washizu elements with the possibility of very large load steps in nonlinear applications. Another essential advantage of present development is the application to FE2 computations where the computing times are dominated by the solution of the micro problems at the shell integration points. Depending on the used interpolation for the shell strains the new element is approximately by a factor 4 or 9 faster than the corresponding version with full integration.

Keywords Reissner–Mindlin shell theory · Hu–Washizu variational principle · One point integration and physical hourglass stabilization · High accuracy for coarse and distorted meshes · Possibility of very large load steps · Fast stiffness computation

1 Introduction

Nonlinear structural analysis of thin structures requires effective and robust element formulations. Especially the possibility of large solution steps and high accuracy when using reasonable unstructured meshes are desired properties.

To bypass the difficulties caused by C^1–requirements of the Kirchhoff–Love theory many of the shell models consider transverse shear deformations within a Reissner–Mindlin theory. Low order elements like quadrilaterals using a standard displacement interpolation are characterized by locking phenomena and lead to unacceptable stiff results when reasonable refined finite element meshes are employed. In shells two types of locking occur: transverse shear locking in which bending modes are excluded and nearly all energy is stored in transverse shear terms, and membrane locking in which bending energy is restrained and energy is stored in membrane terms. In the following only 4-node Reissner–Mindlin shell elements are discussed.

An effective method to avoid transverse shear locking is based on assumed shear strains first proposed in Ref. [1], and subsequently extended among others in [2–4]. The assumed strain method has also been applied to approximate the membrane strains, e.g. [5–7]. The basis for these methods are multi-field variational principles. Especially for linear elasticity the Hellinger–Reissner functional is adequate as variational foundation for mixed elements, e.g. [8, 9]. In case of nonlinear material laws a local iteration for the determination of the physical strains is necessary. Hence, a Hu–Washizu functional with independent displacements, stresses and strains seems to be more appropriate, e.g. [10–

✉ Werner Wagner
werner.wagner@kit.edu

Friedrich Gruttmann
gruttmann@mechanik.tu-darmstadt.de

[1] Institut für Mechanik, Technische Universität Darmstadt, Franziska-Braun-Str. 7, 64287 Darmstadt, Germany

[2] Institut für Baustatik, Karlsruhe Institute of Technology, Kaiserstr. 12, 76131 Karlsruhe, Germany

Published online: 11 April 2025

18]. Within the so–called enhanced strain formulation the assumed stresses are eliminated from the set of equations using orthogonality conditions and a two field formulation remains, [19, 20]. This approach has been successfully applied for shell problems in a multiplicity of publications.

One point quadrature of 4-node shell elements have been first developed by Belytschko et al. [21, 22]. These type of elements have to be stabilized to avoid so–called hourglass modes. In [23] a resultant-stress degenerated shell element is presented. The approach permits use of three-dimensional constitutive equations. The kinematics are improved such that the element [24] is accurate for warped configurations. A nodal projection is added and as a result the element passes the quadratic transverse-deflection patch test. The application of empirical problem dependent parameters was abandoned in [25] with the construction of a physical stabilization control. Some correction terms lead to coupling of the membrane strains with the rotations. Without the correction the element undergoes artificial membrane strains due to rigid body rotations in case of warped configurations. Furthermore, the interpolation functions [4] are incorporated to approximate the transverse shear strain. For nonlinear explicit dynamics two further assumptions are made. Based on above publications the authors of [26] include so-called drilling rotations into the formulation. This allows the assembly with spatial beams or the discretization of intersecting shells. In [27] an unidimensional tangent modulus is used in order to compute the stabilization forces for non-linear material behavior.

A general purpose shell element for nonlinear applications including sheet metal forming simulation is developed based on reduced integration with one point quadrature in [28]. The rigid body projection is introduced to treat rigid body rotations effectively. Through-thickness deformation is included in [29] leading to a 7-parameter theory. Thereby thickness change and also a linear variation of thickness stretch is accounted for. The formulation [30] takes coupling between the hourglass field and enhanced assumed strain variables into consideration. With improvement of the membrane formulation the elements passes the patch tests [31]. The Hellinger-Reissner principle is the variational foundation of the one point integrated shell element [32]. A reduced integrated and stabilized version of the MITC4+ element [33, 34] is recently proposed in [35]. The developed degenerated shell element is implemented into an implicit static and explicit dynamic finite element code.

In most of the above discussed papers the underlying Hu–Washizu variational functional is applied in a special form. The assumed stress field is chosen orthogonal to the difference between the interpolated strain and the standard strain and a two-field variational formulation as in the enhanced strain method remains [19, 20].

Another possibility to analyze shell structures is the use of one point integrated solid elements with hourglass stabilization [36–38]. In [39] the Taylor expansion of the Second Piola-Kirchhoff stress tensor is performed. For inelastic problems a secant modulus is used to define an artificial hourglass shear modulus.

The essential features and new aspects of present formulation are as follows:

(i) We apply the kinematic assumptions of the nonlinear Reissner–Mindlin shell theory. The variational formulation is based on a Hu–Washizu functional with independent displacements, stress resultants and shell strains. In contrast to existing approaches the assumed stress resultants are not eliminated using some orthogonality conditions.

(ii) The finite element formulation for 4–node elements is specified, where the ansatz functions for the independent quantities are taken from our previous publications [11–13]. The element has the standard 5 or 6 degrees of freedom at the nodes, possesses the correct rank and fulfills the membrane and bending patch test. It can be applied to linear and nonlinear shell problems with kinks or intersections. The element is free of locking, thus shows a high accuracy for coarse and distorted meshes.

(iii) The application of three basic assumptions leads directly to an element formulation with one point quadrature and hourglass stabilization. The input of problem dependent control parameters is not necessary. In contrast to existing approaches no additional projections of some element matrices have to be applied in case of warped elements. In several existing formulations the constant material matrix of the last load increment is used to preserve quadratic convergence in the Newton–Raphson iteration. This leads to a path dependency even for hyperelastic material behavior. In present approach the actual matrix can be used which avoids this unphysical feature.

(iv) The stabilization terms can be integrated analytically. Thereby a series expansion of the geometrical shell strains as well as the associated variation and linearization is performed. The element formulation inherits the well-known robustness of Hu–Washizu elements in nonlinear problems with large deformations. Very large load steps can be applied in comparison with standard displacement elements or enhanced strain elements. The element formulation can be applied to large strain problems. Without further adaptions dynamic shell problems along with explicit or implicit time integration methods can be computed.

(v) With present one point integrated element the computing times can be significantly reduced. This holds

especially for FE2 computations where the computing times are dominated by the solution of the micro problems associated with the integration points of the shell.

2 Hu–Washizu variational formulation

Let $\mathcal{B}$ be the three–dimensional Euclidean space occupied by the shell of thickness h in the reference configuration. With ξ^i we denote a convected coordinate system of the body. The coordinate in thickness direction ξ^3 is bounded by $h^- \leq \xi^3 \leq h^+$, where h^- and h^+ are the coordinates of the outer surfaces. Thus, the reference surface can arbitrarily be chosen. For below computed examples we used the mid surface. In the following the summation convention is used for repeated indices, where Latin indices range from 1 to 3 and Greek indices range from 1 to 2. Commas denote partial differentiation with respect to the coordinates ξ^α. The coordinate on the boundary $\Gamma = \Gamma_u \cup \Gamma_\sigma$ of the initial reference surface Ω is denoted by s.

The position vectors of the initial and current shell reference surface are denoted as $\mathbf{X}(\xi^1, \xi^2)$ and $\mathbf{x}(\xi^1, \xi^2)$, respectively. Hence, the displacement vector of the reference surface is defined with $\mathbf{u} = \mathbf{x} - \mathbf{X}$. A vector field $\mathbf{D}(\xi^1, \xi^2)$ with $|\mathbf{D}(\xi^1, \xi^2)| = 1$, associated with the initial configuration, is introduced. The unit director $\mathbf{d}$ of the current configuration is obtained by an orthogonal transformation of the initial vector $\mathbf{D}$. With $\mathbf{x}_{,\alpha} \cdot \mathbf{d} \neq 0$ shear deformations are accounted for within the Reissner–Mindlin theory.

The shell is loaded statically by surface loads $\bar{\mathbf{p}}$ on Ω as well as by boundary loads $\bar{\mathbf{t}}$ on the boundary Γ_σ. The loads are assumed to be independent of the displacements. Hence, the variational foundation using the Hu–Washizu functional reads

$$\begin{aligned}\Pi(\mathbf{v}, \boldsymbol{\sigma}, \boldsymbol{\varepsilon}) \;&= \int_\Omega [W(\boldsymbol{\varepsilon}) + \boldsymbol{\sigma}^T(\boldsymbol{\varepsilon}_g(\mathbf{v}) - \boldsymbol{\varepsilon}) - \mathbf{u}^T \bar{\mathbf{p}}]\, \mathrm{d}A \\ &\quad - \int_{\Gamma_\sigma} \mathbf{u}^T \bar{\mathbf{t}}\, \mathrm{d}s \to \text{stat.} \end{aligned} \tag{1}$$

with $\mathbf{v} = [\mathbf{u}, \mathbf{d}]^T$, $\mathrm{d}A = j\, d\xi^1\, d\xi^2$ and $j = |\mathbf{X}_{,1} \times \mathbf{X}_{,2}|$. The geometric shell strains are derived inserting the kinematic assumptions into the covariant components of the Green-Lagrange strain tensor. They are organized in the vector

$$\boldsymbol{\varepsilon}_g(\mathbf{v}) = [\varepsilon_{11}, \varepsilon_{22}, 2\varepsilon_{12}, \kappa_{11}, \kappa_{22}, 2\kappa_{12}, \gamma_1, \gamma_2]^T, \tag{2}$$

where the membrane strains $\varepsilon_{\alpha\beta}$, curvatures $\kappa_{\alpha\beta}$ and transverse shear strains γ_α read

$$\begin{aligned}\varepsilon_{\alpha\beta} &= \frac{1}{2}(\mathbf{x}_{,\alpha} \cdot \mathbf{x}_{,\beta} - \mathbf{X}_{,\alpha} \cdot \mathbf{X}_{,\beta}) \\ \kappa_{\alpha\beta} &= \frac{1}{2}(\mathbf{x}_{,\alpha} \cdot \mathbf{d}_{,\beta} + \mathbf{x}_{,\beta} \cdot \mathbf{d}_{,\alpha} - \mathbf{X}_{,\alpha} \cdot \mathbf{D}_{,\beta} - \mathbf{X}_{,\beta} \cdot \mathbf{D}_{,\alpha}) \\ \gamma_\alpha &= \mathbf{x}_{,\alpha} \cdot \mathbf{d} - \mathbf{X}_{,\alpha} \cdot \mathbf{D}\,. \end{aligned} \tag{3}$$

The strain energy density W is a function of the independent shell strains $\boldsymbol{\varepsilon}$ with components in a sequence as in Eq. (2). In case of linear elasticity it holds $W(\boldsymbol{\varepsilon}) = \frac{1}{2}\boldsymbol{\varepsilon}^T \mathbf{C}\, \boldsymbol{\varepsilon}$ where $\mathbf{C}$ is the constant elasticity matrix. The vector of independent stress resultants

$$\boldsymbol{\sigma} = [n^{11}, n^{22}, n^{12}, m^{11}, m^{22}, m^{12}, q^1, q^2]^T \tag{4}$$

is defined with membrane forces $n^{\alpha\beta} = n^{\beta\alpha}$, bending moments $m^{\alpha\beta} = m^{\beta\alpha}$ and shear forces q^α.

Introducing $\boldsymbol{\theta} := [\mathbf{v}, \boldsymbol{\sigma}, \boldsymbol{\varepsilon}]^T$ and admissible variations $\delta\boldsymbol{\theta} := [\delta\mathbf{v}, \delta\boldsymbol{\sigma}, \delta\boldsymbol{\varepsilon}]^T$ the stationary condition associated with functional (1) reads

$$\begin{aligned}\delta\Pi \;&:= g(\boldsymbol{\theta}, \delta\boldsymbol{\theta}) = \int_\Omega [\delta\boldsymbol{\varepsilon}^T(\partial_{\boldsymbol{\varepsilon}} W - \boldsymbol{\sigma}) + \delta\boldsymbol{\sigma}^T(\boldsymbol{\varepsilon}_g - \boldsymbol{\varepsilon}) \\ &\quad + \delta\boldsymbol{\varepsilon}_g^T \boldsymbol{\sigma}]\, \mathrm{d}A + g_{ext} = 0 \\ g_{ext} \;&= -\int_\Omega \delta\mathbf{u}^T \bar{\mathbf{p}}\, \mathrm{d}A - \int_{\Gamma_\sigma} \delta\mathbf{u}^T \bar{\mathbf{t}}\, \mathrm{d}s\,. \end{aligned} \tag{5}$$

With integration by parts and application of standard arguments of variational calculus one obtains the associated Euler–Lagrange equations. These are the static field equations, the geometric field equations and the constitutive equations in Ω, as well as the static boundary conditions on Γ_σ, see [11].

The associated finite element equations are iteratively solved applying a Newton–Raphson iteration. For this purpose the linearization of the stationary condition (5) is derived with $\mathbf{C} = \partial^2_{\boldsymbol{\varepsilon}} W$ as

$$\begin{aligned}&\mathrm{L}[g(\boldsymbol{\theta}, \delta\boldsymbol{\theta}), \Delta\boldsymbol{\theta}] := g(\boldsymbol{\theta}, \delta\boldsymbol{\theta}) + \mathrm{D}g \cdot \Delta\boldsymbol{\theta} \\ &= g_{ext} + \int_\Omega \Delta\delta\boldsymbol{\varepsilon}_g^T \boldsymbol{\sigma}\, \mathrm{d}A + \int_\Omega \begin{bmatrix} \delta\boldsymbol{\varepsilon}_g \\ \delta\boldsymbol{\sigma} \\ \delta\boldsymbol{\varepsilon} \end{bmatrix}^T \\ &\left\{ \begin{bmatrix} \boldsymbol{\sigma} \\ \boldsymbol{\varepsilon}_g - \boldsymbol{\varepsilon} \\ \partial_{\boldsymbol{\varepsilon}} W - \boldsymbol{\sigma} \end{bmatrix} + \begin{bmatrix} \mathbf{0} & \mathbf{1}_8 & \mathbf{0} \\ \mathbf{1}_8 & \mathbf{0} & -\mathbf{1}_8 \\ \mathbf{0} & -\mathbf{1}_8 & \mathbf{C} \end{bmatrix} \begin{bmatrix} \Delta\boldsymbol{\varepsilon}_g \\ \Delta\boldsymbol{\sigma} \\ \Delta\boldsymbol{\varepsilon} \end{bmatrix} \right\} \mathrm{d}A\,, \end{aligned} \tag{6}$$

where $\mathbf{1}_n$ denotes a unit matrix of order n. The geometric boundary conditions $\mathbf{v} = \bar{\mathbf{v}}$ on Γ_u have to be fulfilled as constraints.

Remark It is important to note that for inelastic material behavior Eq. (1) does not hold, whereas the successive ones are applicable. We keep the notation $\partial_{\boldsymbol{\varepsilon}} W$ for the stress resultants computed from the material law. They are obtained with the respective inelastic material law for the stresses and a thickness integration [11, 40].

3 Finite element equations

The isoparametric concept for 4-node elements using bilinear functions $N_I(\xi,\eta) = \frac{1}{4}(1+\xi_I\,\xi)(1+\eta_I\,\eta)$ is applied. For the coordinates of the unit square holds $-1 \le \{\xi,\eta\} \le 1$ and $\xi_I \in \{-1,1,1,-1\}$, $\eta_I \in \{-1,-1,1,1\}$. The constant orthonormal element coordinate system is denoted by $[\mathbf{t}_1,\mathbf{t}_2,\mathbf{t}_3]$, see [13]. Hence, the Jacobian matrix $\mathbf{J}$ is expressed as

$$\mathbf{J} = \begin{bmatrix} J_{11} & J_{12} \\ J_{21} & J_{22} \end{bmatrix} = \begin{bmatrix} \mathbf{X}^h_{,\xi}\cdot\mathbf{t}_1 & \mathbf{X}^h_{,\xi}\cdot\mathbf{t}_2 \\ \mathbf{X}^h_{,\eta}\cdot\mathbf{t}_1 & \mathbf{X}^h_{,\eta}\cdot\mathbf{t}_2 \end{bmatrix}. \tag{7}$$

The superscript h refers to the finite element approximation of the particular quantity, and commas denote partial derivatives with respect to ξ or η. It holds

$$\begin{aligned} \mathbf{X}^h_{,\xi} &= \mathbf{G}^0_\xi + \eta\,\mathbf{G}^1 & \mathbf{G}^0_\xi &= \frac{1}{4}\sum_{I=1}^{4}\xi_I\,\mathbf{X}_I \\ \mathbf{X}^h_{,\eta} &= \mathbf{G}^0_\eta + \xi\,\mathbf{G}^1 & \mathbf{G}^0_\eta &= \frac{1}{4}\sum_{I=1}^{4}\eta_I\,\mathbf{X}_I \\ & & \mathbf{G}^1 &= \frac{1}{4}\sum_{I=1}^{4}\xi_I\,\eta_I\,\mathbf{X}_I\,, \end{aligned} \tag{8}$$

where $\mathbf{X}_I$ denote the nodal position vectors.

The matrix

$$\mathbf{T} = \begin{bmatrix} \mathbf{T}^0 & \mathbf{0} & \mathbf{0} \\ \mathbf{0} & \mathbf{T}^0 & \mathbf{0} \\ \mathbf{0} & \mathbf{0} & \tilde{\mathbf{T}}^0 \end{bmatrix}$$

with

$$\mathbf{T}^0 = \begin{bmatrix} J^0_{11}J^0_{11} & J^0_{21}J^0_{21} & a\,J^0_{11}J^0_{21} \\ J^0_{12}J^0_{12} & J^0_{22}J^0_{22} & a\,J^0_{12}J^0_{22} \\ b\,J^0_{11}J^0_{12} & b\,J^0_{21}J^0_{22} & J^0_{11}J^0_{22}+J^0_{12}J^0_{21} \end{bmatrix} \tag{9}$$

and

$$\tilde{\mathbf{T}}^0 = \begin{bmatrix} J^0_{11} & J^0_{21} \\ J^0_{12} & J^0_{22} \end{bmatrix}$$

causes a transformation of contravariant tensor components to the constant element base system $\mathbf{t}_i$. The entries $J^0_{\alpha\beta}$ are the components of $\mathbf{J}$ evaluated at the element center. The factors a and b are specified below. Detailed investigations on the use of ansatz functions for contravariant stress *and* strain components in the framework of a Hu–Washizu functional are contained in Ref. [15].

The finite element approximation of the shell strains reads

$$\boldsymbol{\varepsilon}^h_g = \begin{bmatrix} \frac{1}{2}(\mathbf{x}^h_{,1}\cdot\mathbf{x}^h_{,1} - \mathbf{X}^h_{,1}\cdot\mathbf{X}^h_{,1}) \\ \frac{1}{2}(\mathbf{x}^h_{,2}\cdot\mathbf{x}^h_{,2} - \mathbf{X}^h_{,2}\cdot\mathbf{X}^h_{,2}) \\ \mathbf{x}^h_{,1}\cdot\mathbf{x}^h_{,2} - \mathbf{X}^h_{,1}\cdot\mathbf{X}^h_{,2} \\ \mathbf{x}^h_{,1}\cdot\mathbf{d}^h_{,1} - \mathbf{X}^h_{,1}\cdot\mathbf{D}^h_{,1} \\ \mathbf{x}^h_{,2}\cdot\mathbf{d}^h_{,2} - \mathbf{X}^h_{,2}\cdot\mathbf{D}^h_{,2} \\ \mathbf{x}^h_{,1}\cdot\mathbf{d}^h_{,2} + \mathbf{x}^h_{,2}\cdot\mathbf{d}^h_{,1} - \mathbf{X}^h_{,1}\cdot\mathbf{D}^h_{,2} - \mathbf{X}^h_{,2}\cdot\mathbf{D}^h_{,1} \\ \mathbf{J}^{-1}\begin{Bmatrix} \frac{1}{2}[(1-\eta)\,\gamma^B_\xi + (1+\eta)\,\gamma^D_\xi] \\ \frac{1}{2}[(1-\xi)\,\gamma^A_\eta + (1+\xi)\,\gamma^C_\eta] \end{Bmatrix} \end{bmatrix}. \tag{10}$$

With incorporation of the assumed transverse shear strain interpolation [4] using the shear strains of the midside nodes $\gamma^A_\eta, \gamma^B_\xi, \gamma^C_\eta, \gamma^D_\xi$ the bending patch test can be fulfilled [11]. Furthermore, it holds

$$\begin{aligned} \mathbf{x}^h_{,\alpha} &= \sum_{I=1}^{4} N_{I,\alpha}\,(\mathbf{X}_I + \mathbf{u}_I) \qquad \alpha = 1,2 \\ \mathbf{d}^h_{,\alpha} &= \sum_{I=1}^{4} N_{I,\alpha}\,\mathbf{d}_I \end{aligned} \tag{11}$$

with the shape function derivatives $N_{I,\alpha}$ and the nodal vectors $\mathbf{X}_I, \mathbf{u}_I, \mathbf{d}_I$. The nodal director vector $\mathbf{d}_I$ is computed with the initial director $\mathbf{D}_I$ and rotational parameters $\boldsymbol{\varphi}_I$ by orthogonal transformations. The analogues relations hold for $\mathbf{X}^h_{,\alpha}$ and $\mathbf{D}^h_{,\alpha}$.

The finite element approximation of the vector $\delta\boldsymbol{\theta}^h := [\delta\boldsymbol{\varepsilon}^h_g, \delta\boldsymbol{\sigma}^h, \delta\boldsymbol{\varepsilon}^h]^T$ can be written as

$$\begin{bmatrix} \delta\boldsymbol{\varepsilon}^h_g \\ \delta\boldsymbol{\sigma}^h \\ \delta\boldsymbol{\varepsilon}^h \end{bmatrix} = \begin{bmatrix} \mathbf{B} & \mathbf{0} & \mathbf{0} \\ \mathbf{0} & \mathbf{N}_\sigma & \mathbf{0} \\ \mathbf{0} & \mathbf{0} & \mathbf{N}_\varepsilon \end{bmatrix} \begin{bmatrix} \delta\hat{\mathbf{v}} \\ \delta\hat{\boldsymbol{\sigma}} \\ \delta\hat{\boldsymbol{\varepsilon}} \end{bmatrix} \tag{12}$$

$$\delta\boldsymbol{\theta}^h = \mathbf{N}_\theta\,\delta\hat{\boldsymbol{\theta}}\,.$$

The matrix $\mathbf{B}$ with assumed strain interpolation [4] is specified in [11]. The matrix $\mathbf{N}_\sigma$ for the interpolation of $\boldsymbol{\sigma}^h = \mathbf{N}_\sigma\,\hat{\boldsymbol{\sigma}}$ is chosen as

$$\mathbf{N}_\sigma = [\mathbf{N}^1_\sigma, \mathbf{N}^2_\sigma] \qquad \mathbf{N}^1_\sigma = \mathbf{1}_8 \qquad \mathbf{N}^2_\sigma = \mathbf{T}_\sigma\,\mathbf{M}_\sigma$$

with

$$\mathbf{M}_\sigma = \begin{bmatrix} \mathbf{M}^m_\sigma & \mathbf{0} & \mathbf{0} \\ \mathbf{0} & \mathbf{M}^b_\sigma & \mathbf{0} \\ \mathbf{0} & \mathbf{0} & \mathbf{M}^s_\sigma \end{bmatrix} \tag{13}$$

and

$$\mathbf{M}^m_\sigma = \mathbf{M}^b_\sigma = \begin{bmatrix} \eta-\bar{\eta} & 0 \\ 0 & \xi-\bar{\xi} \\ 0 & 0 \end{bmatrix}, \quad \mathbf{M}^s_\sigma = \begin{bmatrix} \eta-\bar{\eta} & 0 \\ 0 & \xi-\bar{\xi} \end{bmatrix},$$

where $\mathbf{T}_\sigma = \mathbf{T}$ with $a = 2$ and $b = 1$.

The constants $\bar{\xi} = \int_{\Omega_e} \xi \, \mathrm{d}A/A_e$ and $\bar{\eta} = \int_{\Omega_e} \eta \, \mathrm{d}A/A_e$ are the coordinates of the center of gravity of an element with area $A_e = \int_{\Omega_e} \mathrm{d}A$ and fulfill

$$\int_{\Omega_e} (\xi - \bar{\xi}) \, \mathrm{d}A = 0 \qquad \int_{\Omega_e} (\eta - \bar{\eta}) \, \mathrm{d}A = 0 \,. \tag{14}$$

These constants are important to obtain decoupled matrices for the one point quadrature. For rectangular elements holds $\bar{\xi} = \bar{\eta} = 0$. The parameter vector $\hat{\boldsymbol{\sigma}} = [\hat{\boldsymbol{\sigma}}_1, \hat{\boldsymbol{\sigma}}_2]^T$ contains 8 parameters for the constant part and 6 parameters for the varying part of the stress resultants. The interpolation of the membrane forces and bending moments corresponds to the membrane part in Ref. [41]. The original approach for plane stress problems was published with $\bar{\xi} = \bar{\eta} = 0$ in Ref. [42].

The matrix $\mathbf{N}_\varepsilon$ for the interpolation of the independent strains $\boldsymbol{\varepsilon}^h = \mathbf{N}_\varepsilon \, \hat{\boldsymbol{\varepsilon}}$, where $\hat{\boldsymbol{\varepsilon}} = [\hat{\boldsymbol{\varepsilon}}_1, \hat{\boldsymbol{\varepsilon}}_2, \hat{\boldsymbol{\varepsilon}}_3]^T$, $\hat{\boldsymbol{\varepsilon}}_1 \in \mathbb{R}^8$, $\hat{\boldsymbol{\varepsilon}}_2 \in \mathbb{R}^6$, $\hat{\boldsymbol{\varepsilon}}_3 \in \mathbb{R}^n$, is chosen as

$$\begin{aligned} &\mathbf{N}_\varepsilon = \left[\mathbf{N}_\varepsilon^1, \mathbf{N}_\varepsilon^2, \mathbf{N}_\varepsilon^3\right] \\ &\mathbf{N}_\varepsilon^1 = \mathbf{1}_8 \qquad \mathbf{N}_\varepsilon^2 = \mathbf{T}_\varepsilon \, \mathbf{M}_\varepsilon^2 \qquad \mathbf{N}_\varepsilon^3 = \mathbf{T}_\varepsilon \, \mathbf{M}_\varepsilon^3 \,, \end{aligned} \tag{15}$$

where $\mathbf{T}_\varepsilon = \mathbf{T}$ with $a = 1, b = 2$. The interpolation matrices are chosen as

$$\begin{aligned} &\mathbf{M}_\varepsilon^2 = \mathbf{M}_\sigma \qquad \mathbf{M}_\varepsilon^3 = \begin{bmatrix} \mathbf{M}_{\varepsilon n}^{3m} \\ \mathbf{0} \\ \mathbf{0} \end{bmatrix}_{8\times n} \\ &\mathbf{M}_{\varepsilon n}^{3m} = \begin{bmatrix} \xi & 0 & 0 & 0 & \xi\,\eta & 0 & 0 & \widehat{\eta} & 0 & \widehat{\xi} & 0 & 0 & 0 \\ 0 & \eta & 0 & 0 & 0 & \xi\,\eta & 0 & 0 & \widehat{\xi} & 0 & \widehat{\eta} & 0 & 0 \\ 0 & 0 & \xi & \eta & 0 & 0 & \xi\,\eta & 0 & 0 & 0 & 0 & \widehat{\eta} & \widehat{\xi} \end{bmatrix}, \end{aligned} \tag{16}$$

where $\widehat{\xi} := \xi\,(\eta^2 - c)$, $\widehat{\eta} := \eta\,(\xi^2 - c)$. The shape factor c considers the deviation of the element geometry from a square [43]. The index $n \in \{0, 2, 4, 7, 9, 11, 13\}$ has the meaning that optionally the first n columns are taken. With $n = 0$ the matrix $\mathbf{N}_\varepsilon^3$ and the related parameter vector $\hat{\boldsymbol{\varepsilon}}_3$ are omitted.

The finite element approximation of the virtual work of $\bar{\mathbf{p}}$ and $\bar{\mathbf{t}}$ leads to

$$g_{ext}^h = -\sum_{e=1}^{numel} \delta\hat{\mathbf{v}}^T \, \mathbf{f}^a. \tag{17}$$

Here, *numel* denotes the total number of finite shell elements to discretize the problem and $\mathbf{f}^a$ corresponds to the load vector of a standard displacement element. Furthermore, it holds

$$\int_\Omega \Delta\delta\boldsymbol{\varepsilon}_g^{hT} \, \boldsymbol{\sigma}^h \, \mathrm{d}A = \sum_{e=1}^{numel} \delta\hat{\mathbf{v}}^T \mathbf{K}_g \Delta\hat{\mathbf{v}} \qquad \mathbf{K}_g = \int_{\Omega_e} \mathbf{K}_\sigma \, \mathrm{d}A \,, \tag{18}$$

where $\mathbf{K}_\sigma$ is specified in detail in Ref. [11].

We now insert $\delta\boldsymbol{\theta}^h = \mathbf{N}_\theta \, \delta\hat{\boldsymbol{\theta}}$ according to Eqs. (12) and the corresponding equation $\Delta\boldsymbol{\theta}^h = \mathbf{N}_\theta \, \Delta\hat{\boldsymbol{\theta}}$ along with Eqs. (17) and (18) into the linearized variational equation (6), which now reads

$$\begin{aligned} &\mathrm{L}\left[g(\boldsymbol{\theta}^h, \delta\boldsymbol{\theta}^h), \Delta\boldsymbol{\theta}^h\right] = \\ &\sum_{e=1}^{numel} \begin{bmatrix} \delta\hat{\mathbf{v}} \\ \delta\hat{\boldsymbol{\sigma}} \\ \delta\hat{\boldsymbol{\varepsilon}} \end{bmatrix}_e^T \left\{ \begin{bmatrix} \mathbf{f}^i - \mathbf{f}^a \\ \mathbf{f}^s \\ \mathbf{f}^e \end{bmatrix} + \begin{bmatrix} \mathbf{K}_g & \mathbf{G}^T & \mathbf{0} \\ \mathbf{G} & \mathbf{0} & \mathbf{F}^T \\ \mathbf{0} & \mathbf{F} & \mathbf{H} \end{bmatrix} \begin{bmatrix} \Delta\hat{\mathbf{v}} \\ \Delta\hat{\boldsymbol{\sigma}} \\ \Delta\hat{\boldsymbol{\varepsilon}} \end{bmatrix} \right\}_e \end{aligned} \tag{19}$$

with

$$\begin{aligned} \mathbf{f}^i &= \int_{\Omega_e} \mathbf{B}^T \boldsymbol{\sigma}^h \, \mathrm{d}A = \mathbf{G}^T \, \hat{\boldsymbol{\sigma}} & \mathbf{F} &= -\int_{\Omega_e} \mathbf{N}_\varepsilon^T \, \mathbf{N}_\sigma \, \mathrm{d}A \\ \mathbf{f}^s &= \int_{\Omega_e} \mathbf{N}_\sigma^T \, \boldsymbol{\varepsilon}_g^h \, \mathrm{d}A + \mathbf{F}^T \, \hat{\boldsymbol{\varepsilon}} & \mathbf{G} &= \int_{\Omega_e} \mathbf{N}_\sigma^T \, \mathbf{B} \, \mathrm{d}A \\ \mathbf{f}^e &= \int_{\Omega_e} \mathbf{N}_\varepsilon^T \, \partial_{\boldsymbol{\varepsilon}} W \, \mathrm{d}A + \mathbf{F} \, \hat{\boldsymbol{\sigma}} & \mathbf{H} &= \int_{\Omega_e} \mathbf{N}_\varepsilon^T \, \mathbf{C} \, \mathbf{N}_\varepsilon \, \mathrm{d}A \,. \end{aligned} \tag{20}$$

Let $\mathrm{L}[g(\boldsymbol{\theta}^h, \delta\boldsymbol{\theta}^h), \Delta\boldsymbol{\theta}^h] = 0$ with $\delta\hat{\boldsymbol{\theta}}_e = [\delta\hat{\mathbf{v}}, \delta\hat{\boldsymbol{\sigma}}, \delta\hat{\boldsymbol{\varepsilon}}]_e^T \neq \mathbf{0}$. One obtains for each element the set of equations

$$\begin{bmatrix} \mathbf{K}_g & \mathbf{G}^T & \mathbf{0} \\ \mathbf{G} & \mathbf{0} & \mathbf{F}^T \\ \mathbf{0} & \mathbf{F} & \mathbf{H} \end{bmatrix} \begin{bmatrix} \Delta\hat{\mathbf{v}} \\ \Delta\hat{\boldsymbol{\sigma}} \\ \Delta\hat{\boldsymbol{\varepsilon}} \end{bmatrix} + \begin{bmatrix} \mathbf{f}^i - \mathbf{f}^a \\ \mathbf{f}^s \\ \mathbf{f}^e \end{bmatrix} = \begin{bmatrix} \mathbf{r} \\ \mathbf{0} \\ \mathbf{0} \end{bmatrix}. \tag{21}$$

At equilibrium states holds $\mathbf{f}^s = \mathbf{f}^e = \mathbf{0}$. The vector of element nodal forces $\mathbf{r}$ cancels out with the assembly.

4 One point quadrature and stabilization

One key aspect of the one point quadrature is the vector $\mathbf{f}^e = [\mathbf{f}_1^e, \mathbf{f}_2^e, \mathbf{f}_3^e]^T$ according to Eq. (20). Three basic assumptions are made:

$$\begin{aligned} &1. \quad \mathbf{f}_i^e = \mathbf{0}, \; i = 2, 3 \quad \text{within each iteration step} \\ &2. \quad \partial_{\boldsymbol{\varepsilon}} W = \text{constant within an element} \\ &3. \quad \int_{\Omega_e} \boldsymbol{\varepsilon}_g^h \, \mathrm{d}A = A_e \, \boldsymbol{\varepsilon}_{g0} \quad \boldsymbol{\varepsilon}_{g0} = \boldsymbol{\varepsilon}_g^h(\xi = \eta = 0) \end{aligned} \tag{22}$$

From $(22)_3$ follow the corresponding equations for the virtual strains $\delta\boldsymbol{\varepsilon}_g^h = \mathbf{B} \, \delta\hat{\mathbf{v}}$, the linearized strains $\Delta\boldsymbol{\varepsilon}_g^h = \mathbf{B} \, \Delta\hat{\mathbf{v}}$ and

the expression $\Delta\delta\boldsymbol{\varepsilon}_g^{hT}\boldsymbol{\sigma}^h = \delta\hat{\mathbf{v}}^T\mathbf{K}_\sigma\Delta\hat{\mathbf{v}}$ for the linearized virtual strains. Thus, it holds

$$\int_{\Omega_e}\mathbf{B}\,\mathrm{d}A = A_e\,\mathbf{B}_0 \qquad \mathbf{B}_0 = \mathbf{B}(\xi=\eta=0)$$
$$\int_{\Omega_e}\mathbf{K}_\sigma\,\mathrm{d}A = A_e\,\mathbf{K}_{\sigma 0} \qquad \mathbf{K}_{\sigma 0} = \mathbf{K}_\sigma(\xi=\eta=0)\,. \tag{23}$$

From $(22)_2$ follows $\mathbf{C} = \partial^2_{\boldsymbol{\varepsilon}}W$ = constant within an element. The assumption $(22)_1$ and $\mathbf{C}$ = constant lead with Eq. (14) to decoupling in the matrix $\mathbf{H} = \mathbf{H}^T$, thus $\mathbf{H}_{12} = \mathbf{H}_{13} = \mathbf{0}$. Concerning the structure of $\mathbf{F}$ we refer to the discussion in [13].

The vectors and matrices $(18)_2$ and (20) are now expressed with (13–16) and (22–23)

$$\mathbf{F} = \begin{bmatrix}\mathbf{F}_{11} & \mathbf{0}\\ \mathbf{0} & \mathbf{F}_{22}\\ \mathbf{0} & \mathbf{0}\end{bmatrix} \qquad \begin{aligned}\mathbf{F}_{11} &= -A_e\,\mathbf{1}_8\\ \mathbf{F}_{22} &= -\int_{\Omega_e}\mathbf{N}_\varepsilon^{2T}\,\mathbf{N}_\sigma^2\,\mathrm{d}A\end{aligned}$$

$$\mathbf{H} = \begin{bmatrix}\mathbf{H}_{11} & \mathbf{0} & \mathbf{0}\\ \mathbf{0} & \mathbf{H}_{22} & \mathbf{H}_{23}\\ \mathbf{0} & \mathbf{H}_{32} & \mathbf{H}_{33}\end{bmatrix} \qquad \begin{aligned}\mathbf{H}_{11} &= A_e\,\mathbf{C}\\ \mathbf{H}_{ij} &= \int_{\Omega_e}\mathbf{N}_\varepsilon^{iT}\,\mathbf{C}\,\mathbf{N}_\varepsilon^{j}\,\mathrm{d}A\quad i,j=2,3\end{aligned}$$

$$\mathbf{G} = \begin{bmatrix}\mathbf{G}_1\\ \mathbf{G}_2\end{bmatrix} \qquad \begin{aligned}\mathbf{G}_1 &= A_e\,\mathbf{B}_0\\ \mathbf{G}_2 &= \int_{\Omega_e}\mathbf{N}_\sigma^{2T}\,\mathbf{B}\,\mathrm{d}A\end{aligned}$$

$$\mathbf{K}_g = \mathbf{K}_{g1} + \mathbf{K}_{g2} \qquad \begin{aligned}\mathbf{K}_{g1} &= A_e\,\mathbf{K}_{\sigma 0}\\ \mathbf{K}_{g2} &= \int_{\Omega_e}\mathbf{K}_\sigma(\boldsymbol{\sigma}^h)\,\mathrm{d}A\\ \boldsymbol{\sigma}^h &= \mathbf{N}_\sigma^2\,\hat{\boldsymbol{\sigma}}_2\end{aligned}$$

$$\mathbf{f}^i = \begin{bmatrix}\mathbf{f}_1^i\\ \mathbf{f}_2^i\end{bmatrix} \qquad \begin{aligned}\mathbf{f}_1^i &= A_e\,\mathbf{B}_0^T\,\hat{\boldsymbol{\sigma}}_1\\ \mathbf{f}_2^i &= \mathbf{G}_2^T\,\hat{\boldsymbol{\sigma}}_2\end{aligned}$$

$$\mathbf{f}^e = \begin{bmatrix}\mathbf{f}_1^e\\ \mathbf{f}_2^e\\ \mathbf{f}_3^e\end{bmatrix} \qquad \begin{aligned}\mathbf{f}_1^e &= A_e\,(\partial_{\boldsymbol{\varepsilon}}W - \hat{\boldsymbol{\sigma}}_1)\\ \mathbf{f}_2^e &= \mathbf{0}\\ \mathbf{f}_3^e &= \mathbf{0}\end{aligned}$$

$$\mathbf{f}^s = \begin{bmatrix}\mathbf{f}_1^s\\ \mathbf{f}_2^s\end{bmatrix} \qquad \begin{aligned}\mathbf{f}_1^s &= A_e(\boldsymbol{\varepsilon}_{g0} - \hat{\boldsymbol{\varepsilon}}_1)\\ \mathbf{f}_2^s &= \int_{\Omega_e}\mathbf{N}_\sigma^{2T}\,\boldsymbol{\varepsilon}_g^h\,\mathrm{d}A + \mathbf{F}_{22}^T\,\hat{\boldsymbol{\varepsilon}}_2\,.\end{aligned} \tag{24}$$

The integrals in (24) can be integrated analytically, see Appendix A. For this purpose the series expansion of the geometrical membrane strains and curvatures up to linear terms in ξ and η is derived. Hence, positive whole-number powers of the coordinates ξ and η appear in the integrands. With the associated variation and linearization this is done in an analogues way for the corresponding submatrices in $\mathbf{B}$ and $\mathbf{K}_\sigma$. The alternative is a numerical Gauss integration. Depending on the number of interpolation functions n in Eq. (16) a 2×2 or 3×3 integration is necessary. In this case the series expansion is not necessary.

The incremental strains $\Delta\hat{\boldsymbol{\varepsilon}}_3$ are eliminated from $\mathbf{F}\,\Delta\hat{\boldsymbol{\sigma}} + \mathbf{H}\,\Delta\hat{\boldsymbol{\varepsilon}} + \mathbf{f}^e = \mathbf{0}$ by static condensation

$$\begin{bmatrix}\mathbf{F}_{11} & \mathbf{0}\\ \mathbf{0} & \mathbf{F}_{22}\\ \mathbf{0} & \mathbf{0}\end{bmatrix}\begin{bmatrix}\Delta\hat{\boldsymbol{\sigma}}_1\\ \Delta\hat{\boldsymbol{\sigma}}_2\end{bmatrix} + \begin{bmatrix}\mathbf{H}_{11} & \mathbf{0} & \mathbf{0}\\ \mathbf{0} & \mathbf{H}_{22} & \mathbf{H}_{23}\\ \mathbf{0} & \mathbf{H}_{32} & \mathbf{H}_{33}\end{bmatrix}\begin{bmatrix}\Delta\hat{\boldsymbol{\varepsilon}}_1\\ \Delta\hat{\boldsymbol{\varepsilon}}_2\\ \Delta\hat{\boldsymbol{\varepsilon}}_3\end{bmatrix} + \begin{bmatrix}\mathbf{f}_1^e\\ \mathbf{0}\\ \mathbf{0}\end{bmatrix} = \begin{bmatrix}\mathbf{0}\\ \mathbf{0}\\ \mathbf{0}\end{bmatrix} \tag{25}$$

which leads with

$$\Delta\hat{\boldsymbol{\varepsilon}}_3 = -\mathbf{H}_{33}^{-1}\,\mathbf{H}_{32}\,\Delta\hat{\boldsymbol{\varepsilon}}_2 \tag{26}$$

and $\bar{\mathbf{H}}_{22} = \mathbf{H}_{22} - \mathbf{H}_{23}\,\mathbf{H}_{33}^{-1}\,\mathbf{H}_{32}$ to

$$\begin{aligned}&\mathbf{F}_1\,\Delta\hat{\boldsymbol{\sigma}} + \mathbf{H}_1\,\Delta\bar{\boldsymbol{\varepsilon}} + \bar{\mathbf{f}}_1^e = \mathbf{0}\\ &\mathbf{F}_1 = \begin{bmatrix}\mathbf{F}_{11} & \mathbf{0}\\ \mathbf{0} & \mathbf{F}_{22}\end{bmatrix},\ \mathbf{H}_1 = \begin{bmatrix}\mathbf{H}_{11} & \mathbf{0}\\ \mathbf{0} & \bar{\mathbf{H}}_{22}\end{bmatrix},\\ &\Delta\hat{\boldsymbol{\sigma}} = \begin{bmatrix}\Delta\hat{\boldsymbol{\sigma}}_1\\ \Delta\hat{\boldsymbol{\sigma}}_2\end{bmatrix},\quad \Delta\bar{\boldsymbol{\varepsilon}} = \begin{bmatrix}\Delta\hat{\boldsymbol{\varepsilon}}_1\\ \Delta\hat{\boldsymbol{\varepsilon}}_2\end{bmatrix},\quad \bar{\mathbf{f}}_1^e = \begin{bmatrix}\mathbf{f}_1^e\\ \mathbf{0}\end{bmatrix}\end{aligned} \tag{27}$$

Hence, Eq. (21) becomes

$$\begin{bmatrix}\mathbf{K}_g & \mathbf{G}^T & \mathbf{0}\\ \mathbf{G} & \mathbf{0} & \mathbf{F}_1^T\\ \mathbf{0} & \mathbf{F}_1 & \mathbf{H}_1\end{bmatrix}\begin{bmatrix}\Delta\hat{\mathbf{v}}\\ \Delta\hat{\boldsymbol{\sigma}}\\ \Delta\bar{\boldsymbol{\varepsilon}}\end{bmatrix} + \begin{bmatrix}\mathbf{f}^i - \mathbf{f}^a\\ \mathbf{f}^s\\ \bar{\mathbf{f}}_1^e\end{bmatrix} = \begin{bmatrix}\mathbf{r}\\ \mathbf{0}\\ \mathbf{0}\end{bmatrix}. \tag{28}$$

Since the stresses and strains are interpolated discontinuously across the element boundaries the parameters $\Delta\bar{\boldsymbol{\varepsilon}}$ and $\Delta\hat{\boldsymbol{\sigma}}$ can be eliminated from the set of equations

$$\begin{aligned}\Delta\hat{\boldsymbol{\sigma}} &= -\mathbf{F}_1^{-1}\,(\mathbf{H}_1\,\Delta\bar{\boldsymbol{\varepsilon}} + \bar{\mathbf{f}}_1^e)\\ \Delta\bar{\boldsymbol{\varepsilon}} &= -\mathbf{F}_1^{-T}\,(\mathbf{G}\,\Delta\hat{\mathbf{v}} + \mathbf{f}^s)\,.\end{aligned} \tag{29}$$

Due to the special structure of $\mathbf{F}_1$ the inverse matrix can easily be computed. Only submatrices of order two have to be inverted. Equations (29) are inserted into (28) to obtain

$\mathbf{K}_T^e\ \Delta\hat{\mathbf{v}} + \hat{\mathbf{f}} = \mathbf{r}$. With

$$\begin{aligned}\hat{\mathbf{H}} &= \mathbf{F}_1^{-1}\,\mathbf{H}_1\,\mathbf{F}_1^{-T} = \begin{bmatrix}\hat{\mathbf{H}}_{11} & \mathbf{0}\\ \mathbf{0} & \hat{\mathbf{H}}_{22}\end{bmatrix}\\ \hat{\mathbf{H}}_{11} &= \mathbf{F}_{11}^{-1}\,\mathbf{H}_{11}\,\mathbf{F}_{11}^{-T} = \tfrac{1}{A_e}\mathbf{C}\\ \hat{\mathbf{H}}_{22} &= \mathbf{F}_{22}^{-1}\,\bar{\mathbf{H}}_{22}\,\mathbf{F}_{22}^{-T}\end{aligned} \tag{30}$$

one gets the tangential element stiffness matrix

$$\begin{aligned}\mathbf{K}_T^e &= \mathbf{G}^T\,\hat{\mathbf{H}}\,\mathbf{G} + \mathbf{K}_g\\ &= \mathbf{G}_1^T\,\hat{\mathbf{H}}_{11}\,\mathbf{G}_1 + \mathbf{G}_2^T\,\hat{\mathbf{H}}_{22}\,\mathbf{G}_2 + \mathbf{K}_g\\ &= A_e\,\mathbf{B}_0^T\,\mathbf{C}\,\mathbf{B}_0 + \mathbf{K}_{\text{stab}} + \mathbf{K}_g\end{aligned} \tag{31}$$

as sum of the one point integrated part $A_e\,\mathbf{B}_0^T\,\mathbf{C}\,\mathbf{B}_0$, the stabilization matrix $\mathbf{K}_{\text{stab}} = \mathbf{G}_2^T\,\hat{\mathbf{H}}_{22}\,\mathbf{G}_2$ and the geometrical matrix $\mathbf{K}_g = \mathbf{K}_{g1} + \mathbf{K}_{g2}$. The sum $A_e\,\mathbf{B}_0^T\,\mathbf{C}\,\mathbf{B}_0 + \mathbf{K}_{g1}$ corresponds to the tangential element stiffness matrix of a displacement element computed by one point quadrature. Without the stabilization the element stiffness matrix holds 12 zero eigenvalues. With stabilization the matrix possesses with six zero eigenvalues the correct rank, see Sect. 5.1.

The element residual vector yields

$$\begin{aligned}\hat{\mathbf{f}} &= \mathbf{G}^T(\hat{\boldsymbol{\sigma}} + \hat{\mathbf{H}}\,\mathbf{f}^s - \mathbf{F}_1^{-1}\,\bar{\mathbf{f}}_1^e) - \mathbf{f}^a\\ &= \mathbf{G}_1^T(\hat{\boldsymbol{\sigma}}_1 + \hat{\mathbf{H}}_{11}\,\mathbf{f}_1^s - \mathbf{F}_{11}^{-1}\,\mathbf{f}_1^e) + \mathbf{G}_2^T(\hat{\boldsymbol{\sigma}}_2 + \hat{\mathbf{H}}_{22}\,\mathbf{f}_2^s) - \mathbf{f}^a\\ &= A_e\,\mathbf{B}_0^T\,[\hat{\boldsymbol{\sigma}}_1 + \mathbf{C}\,(\boldsymbol{\varepsilon}_{g0} - \hat{\boldsymbol{\varepsilon}}_1) + (\partial_{\boldsymbol{\varepsilon}} W - \hat{\boldsymbol{\sigma}}_1)]\\ &\quad + \mathbf{G}_2^T\,(\hat{\boldsymbol{\sigma}}_2 + \hat{\mathbf{H}}_{22}\,\mathbf{f}_2^s) - \mathbf{f}^a\\ &= A_e\,\mathbf{B}_0^T\,[\partial_{\boldsymbol{\varepsilon}} W + \mathbf{C}\,(\boldsymbol{\varepsilon}_{g0} - \hat{\boldsymbol{\varepsilon}}_1)] + \mathbf{G}_2^T\,\hat{\mathbf{H}}_{22}\,\mathbf{f}_2^s + \mathbf{f}_{\text{stab}} - \mathbf{f}^a\end{aligned} \tag{32}$$

The sum $A_e\,\mathbf{B}_0^T\,\partial_{\boldsymbol{\varepsilon}} W - \mathbf{f}^a$ corresponds to the element residual vector of a one point integrated displacement element. The terms $\mathbf{C}\,(\boldsymbol{\varepsilon}_{g0} - \hat{\boldsymbol{\varepsilon}}_1)$ and $\mathbf{G}_2^T\,\hat{\mathbf{H}}_{22}\,\mathbf{f}_2^s$ vanish at an equilibrium configuration. Within the Newton iteration they lead along with the associated parts of $\mathbf{K}_T^e$ to the superior convergence behavior of a Hu–Washizu element with the possibility of very large load steps in comparison with a displacement element or an enhanced strain element. In this context we refer to the detailed investigations in Refs. [11, 12]. It should be noted that in this respect also measures can be taken to improve the robustness of displacement based elements and enhanced strain elements [44, 45]. The vector $\mathbf{f}_{\text{stab}} = \mathbf{G}_2^T\,\hat{\boldsymbol{\sigma}}_2$ is crucial for the element stabilization at equilibrium states. For implicit time integration methods in dynamic computations $\mathbf{K}_T^e$ and $\hat{\mathbf{f}}$ are unaltered used to setup the effective stiffness matrix and the effective right hand side. For explicit time integration methods only $\hat{\mathbf{f}}$ is exploited for each element.

The update of the parameters $\hat{\boldsymbol{\sigma}} \Leftarrow \hat{\boldsymbol{\sigma}} + \Delta\hat{\boldsymbol{\sigma}}$ and $\hat{\boldsymbol{\varepsilon}} \Leftarrow \hat{\boldsymbol{\varepsilon}} + \Delta\hat{\boldsymbol{\varepsilon}}$ with $\Delta\hat{\boldsymbol{\sigma}} = [\Delta\hat{\boldsymbol{\sigma}}_1, \Delta\hat{\boldsymbol{\sigma}}_2]^T$, $\Delta\hat{\boldsymbol{\varepsilon}} = [\Delta\hat{\boldsymbol{\varepsilon}}_1, \Delta\hat{\boldsymbol{\varepsilon}}_2, \Delta\hat{\boldsymbol{\varepsilon}}_3]^T$ is performed using Eqs. (29) and (26). For this purpose the necessary matrices for it have to be stored or to be recomputed. The shell elements possess ndf = 5 or 6 degrees of freedom (dofs) at the nodes. At nodes on kinks or intersections 6 dofs (3 global displacements and 3 global rotations) and at the remaining nodes 5 dofs (3 global displacements and 2 local rotations) are present.

Table 1 Used element labels

DISP-FI	Displacement element with full integration
DISP-RI	Displacement element with one point integration without stabilization
HW-FI	Hu–Washizu element with full integration
HW-RI	Hu–Washizu element with one point integration and stabilization

Remark In the publications of Belytschko et al. [21–25] the so-called gamma stabilization technique has been used to setup $\mathbf{K}_{\text{stab}}$ and $\mathbf{f}_{\text{stab}}$. From our knowledge it is not possible to establish a connection to present representation of the stabilization terms.

5 Examples

The derived element formulation is implemented in an extended version of the general purpose finite element program FEAP [46]. If not explicitly stated, the computations are carried out with $n = 13$, thus the complete matrix $\mathbf{N}_\varepsilon^3$ according to Eqs. (15) and (16) is considered. For all examples with homogeneous material the shear correction factor $\kappa = 5/6$ is used. In below presented diagrams the solutions are labeled with the abbreviations according to Table 1, where for the Hu–Washizu element full integration means a 2×2 integration for $n \leq 7$ and a 3×3 integration for $n > 7$. All element versions use the transverse shear approximations [4]. The displacement element DISP-FI corresponds to the MITC4 element.

5.1 Eigenvalue analysis of the element stiffness matrix

At first, we compute the eigenvalues of the linear element stiffness matrix. Following Ref. [17] we examine a square element and a distorted (warped) element with $a = 2,\ h = 0.02,\ E = 10^8,\ \nu = 0.3$, see Fig. 1.

The element stiffness matrix is of order 20. Both versions –the one point integrated and the fully integrated element– lead to six zero eigenvalues corresponding to the six rigid body modes. The remaining 14 nonzero eigenvalues are depicted in Fig. 2.

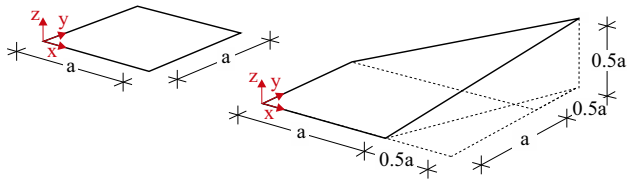

Fig. 1 Element shapes for the eigenvalue analysis

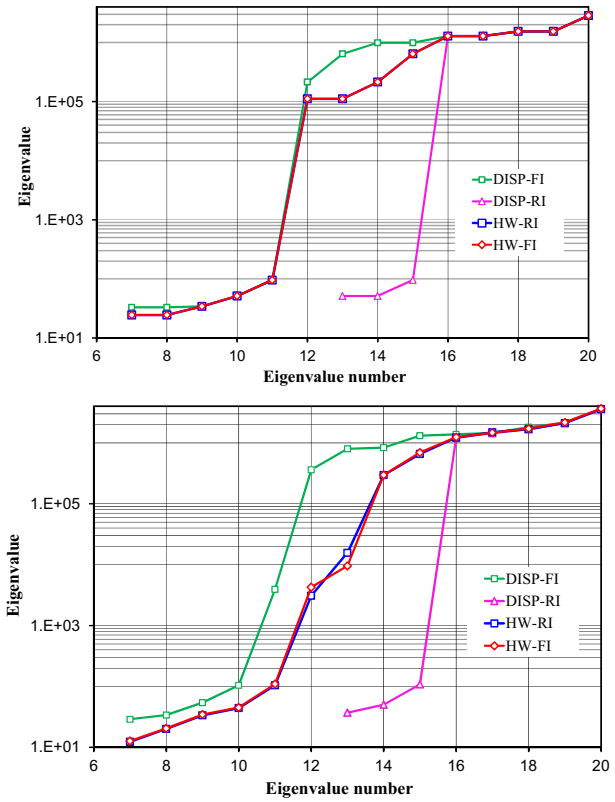

Fig. 2 Eigenvalues of the square element (top) and the distorted element (bottom)

Lower eigenvalues relate to the bending modes, and higher eigenvalues relate to the stiffer membrane- and shear modes. They are divided by a pronounced jump, see Fig. 2. Both versions lead to nearly the same results, whereas the eigenvalues of the displacement element DISP-FI are partly considerable larger. This is the reason for the stiff behavior in the following test examples. Furthermore, results for the one point integrated element without stabilization (DISP-RI) are included. Then twelve zero eigenvalues occur.

Finally, the pure membrane case considering a flat element ($z \equiv 0$) is investigated. The distortion in the $x - y$ plane corresponds to Fig. 1. The out-of plane displacements and the rotations are fixed. The remaining degrees of freedom are 8 in–plane displacements. Hence there are 3 zero eigenvalues associated with the 3 rigid body movements of a flat sheet. As Fig. 3 shows, two further eigenvalues are very small, which

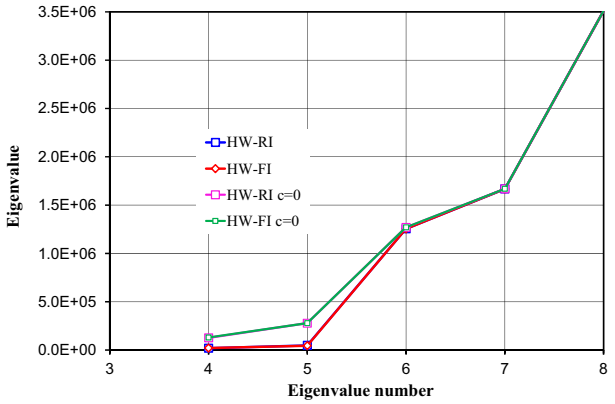

Fig. 3 Eigenvalues of the distorted flat element

is not the case for $c = 0$. Thus, for problems with dominating membrane deformations $c = 0$ should be used to avoid an unstable element behavior.

5.2 Membrane and bending patch test

We investigate the element behavior within a constant membrane and bending patch test as it is depicted in Fig. 4, see also [47]. A rectangular plate of length a and width b is supported at the three corners. We consider in-plane loading and bending loading denoted by load case 1 and 2, respectively. Both, membrane and bending patch test are fulfilled with constant normal forces $n_x = 1, n_y = n_{xy} = 0$ (load case 1) and constant bending moments $m_x = m_y = m_{xy} = 1$ (load case 2) by present element.

5.3 Cook's problem

We consider the nonlinear behavior of the well-known Cook's membrane, first introduced in [20]. It is a tapered panel clamped on one end and uniformly loaded with a resultant $P = 1$ on the other end, see Fig. 5.

Geometrical and material data are $h = 1$ and $E = 2,\ \nu = 1/3$. The problem provides a pure membrane test including element distortions and is a test for handling the in-plane bending dominated by shear. The discretization is performed with a $N \times N$ mesh. For the displacement u_{yA} we depict the performance in dependence of N in Table 2 and Fig. 6. Using present element the total load $P = 1$ can be applied in one step with 6 iterations. Findings for MITC4, MITC4+ and +HW are taken from Table 3 in Ref. [17]. Table 2 contains also results for geometrical linear strains, see also Ref. [48].

The convergence behavior of the MITC4 and MITC4+ elements is relative slow. Solutions for +HW ([17]) and present element exhibit a fast convergence. As already mentioned in above eigenvalue analysis the quadratic shape functions (16) can only be used with $c = 0$. Otherwise the element formu-

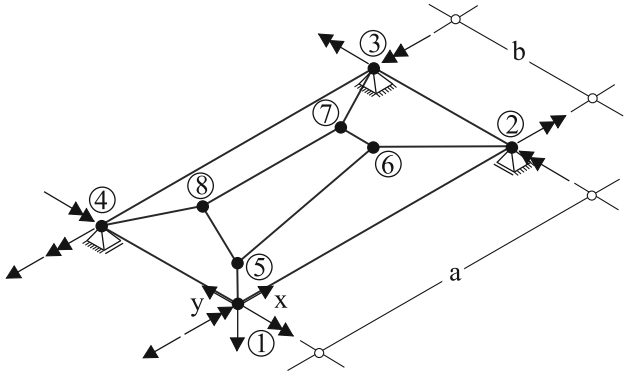

$a = 40$ $\quad E = 10^6$
$b = 20$ $\quad \nu = 0.3$
$h = 0.1$

Load case			1	2		
Node	x	y	$\bar{F}_x$	$\bar{F}_z$	$\bar{m}_x$	$\bar{m}_y$
1	0	0	-10	-2	20	-10
2	40	0	0	0	20	10
3	40	20	0	0	-20	10
4	0	20	-10	0	-20	-10
5	5	5				
6	30	10				
7	30	15				
8	10	15				

Fig. 4 Rectangular plate, patch of 5 elements

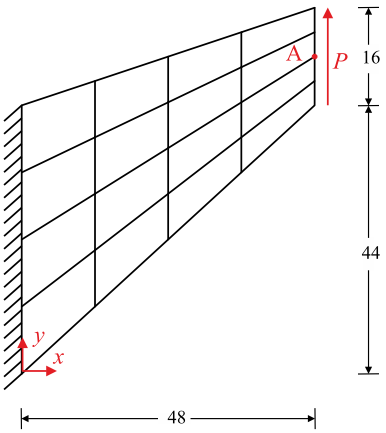

Fig. 5 Cook's problem with a 4×4 mesh

Table 2 Cook's problem: convergence behavior $u_{yA} - N$

FE mesh	4	8	16	32	48
MITC4	7.868	8.960	9.313	9.414	9.435
MITC4+	7.944	8.996	9.329	9.421	9.440
+HW	9.316	9.418	9.448	9.457	9.459
HW-RI c=0	9.451	9.440	9.444	9.450	9.452
HW-RI c=0 geom. linear	12.084	11.996	11.983	11.982	11.982

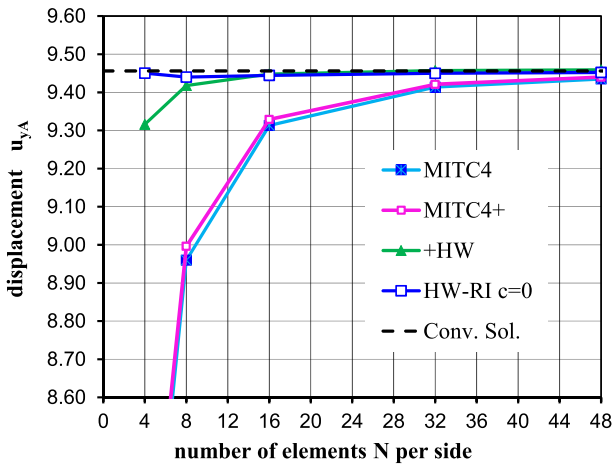

Fig. 6 Cook's problem: convergence behavior $u_{yA} - N$

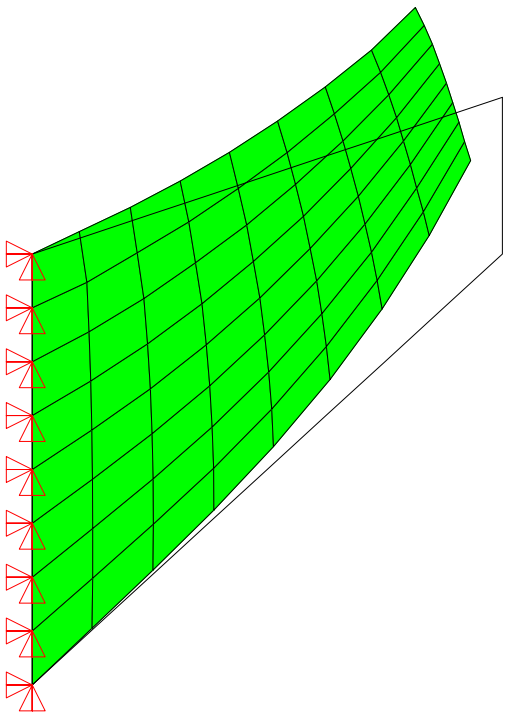

Fig. 7 Cook's problem: deformed mesh for $P = 1$

lation leads in a pure membrane case to hourglassing. The deformed mesh for $P = 1$ is depicted in Fig. 7.

5.4 Twisted beam

We consider the twisted beam problem shown in Fig. 8, originally introduced in [47]. Geometrical and material data are $L = 12$, $b = 1.1$, thickness $h = 0.0032$ and $E = 29 \cdot 10^6$, $\nu = 0.22$, respectively. The beam is clamped at one end and is loaded by an out-of-plane acting load P_y at point A. A regular 4×24 mesh is chosen for the solution.

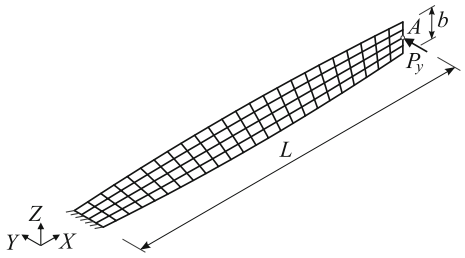

Fig. 8 Twisted beam: geometry and a 4 × 24 regular mesh

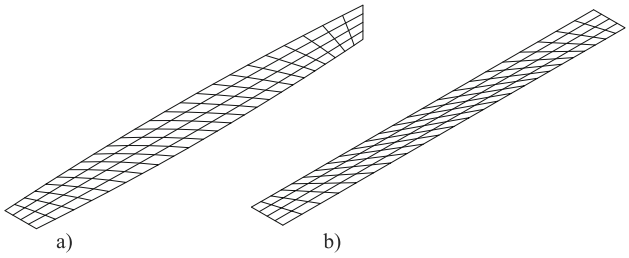

Fig. 10 Twisted beam: distorted 4 × 24 mesh 1, **a** perspective view, **b** perspective view of the flat projection

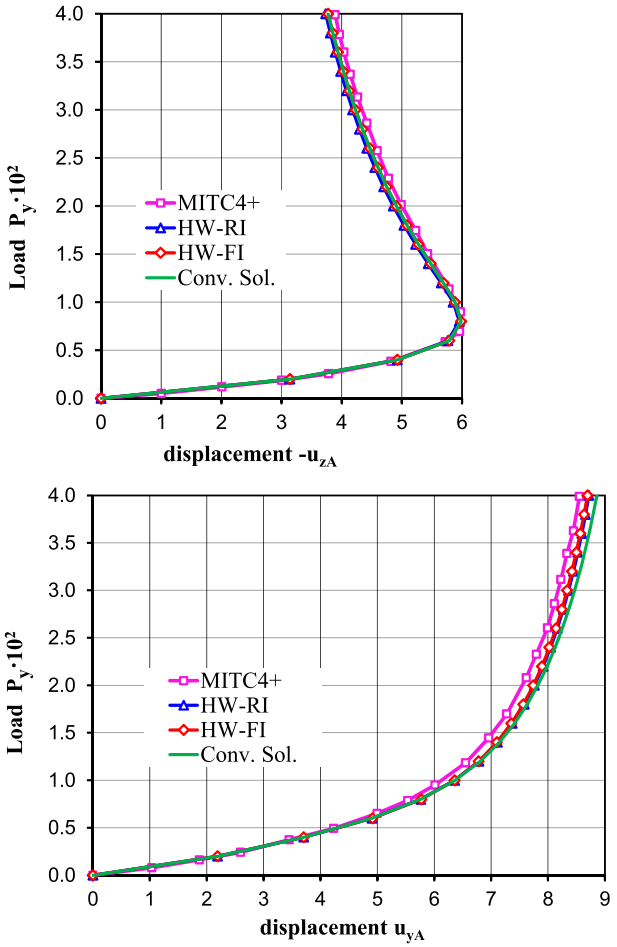

Fig. 9 Twisted beam: $P_y - u_{zA}$ (top) and $P_y - u_{yA}$ (bottom) for the regular 4 × 24 mesh

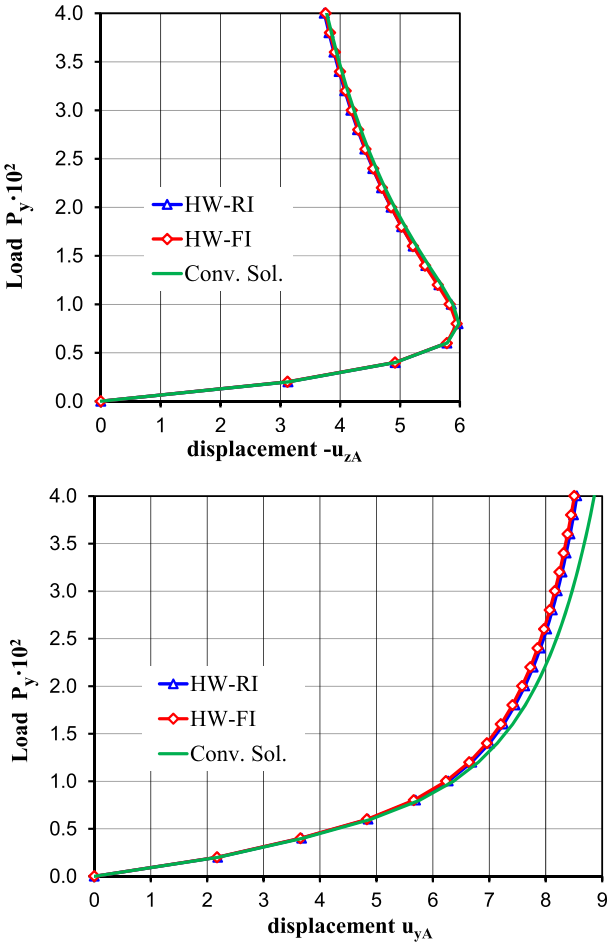

Fig. 11 Twisted beam: $P_y - u_{zA}$ (top) and $P_y - u_{yA}$ (bottom) for the distorted 4 × 24 mesh

Figure 9 depicts the load displacement curves of point A for one point integrated and fully integrated elements as well as results using the MITC4+ element [34]. The converged solution is defined via a 32 × 192 regular mesh.

Furthermore mesh distortion is investigated. The distorted mesh is shown in Fig. 10 together with a flat projection, both in a perspective view. A ratio $L_{max}/L_{min} = 2$ is chosen, where L_{max} and L_{min} denote the longest and shortest element length in the flat projection, respectively.

The associated load displacement curves of point A are contained in Fig. 11. The convergence behavior of the final displacement u_{yA} for the distorted mesh versus the number of elements N in width direction is presented in Fig. 12. The one point integrated element behaves slightly better than the fully integrated element. In addition, the stiff behavior of a pure displacement element is documented.

The deformed beam using the distorted mesh for $P_y = 4 \cdot 10^{-2}$ is depicted in Fig. 13.

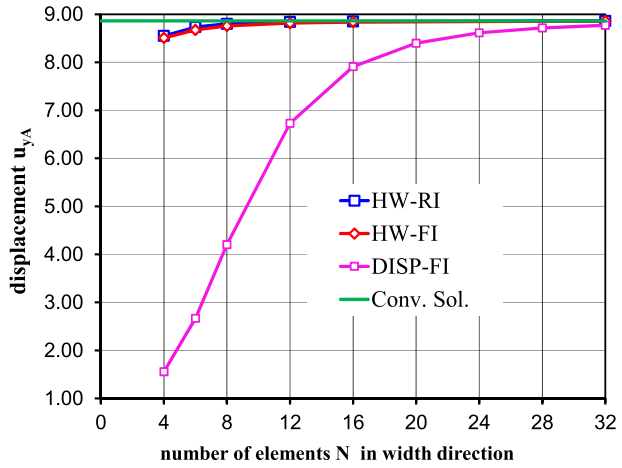

Fig. 12 Twisted beam: $u_{yA} - N$ for the distorted mesh

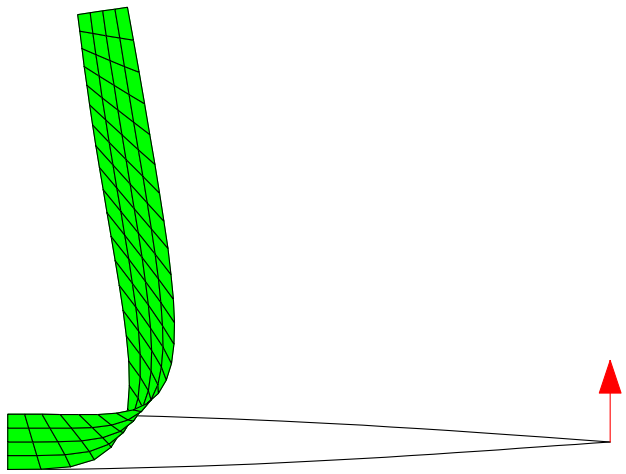

Fig. 13 Twisted beam: deformed beam using the distorted mesh 2 for $P_y = 4 \cdot 10^{-2}$

5.5 Twisted beam-the dynamic case

Four-node quadrilateral shell elements with one quadrature point have been widely used in programs with explicit time integration. Here, we apply present shell formulation without any modification to such a problem class. The above described twisted beam example, see Fig. 8, is modified in the following way: a thickness $h = 0.32$ is chosen, the constant load $P_z(t) = 1$ is now acting in z-direction. A regular 2×12 FE-mesh is the basis of the numerical calculations. Linear dynamic analyses using an explicit time integration ($\Delta T = 0.8 \cdot 10^{-6}\, s$) and an implicit time integration (Newmark, $\Delta T = 1 \cdot 10^{-4}\, s$) are performed. The lumped mass matrix is computed for both methods with the density $\rho = 2.5 \cdot 10^{-4}$. The results are depicted in Fig. 14. A very good agreement with the findings of Ref. [24] can be stated.

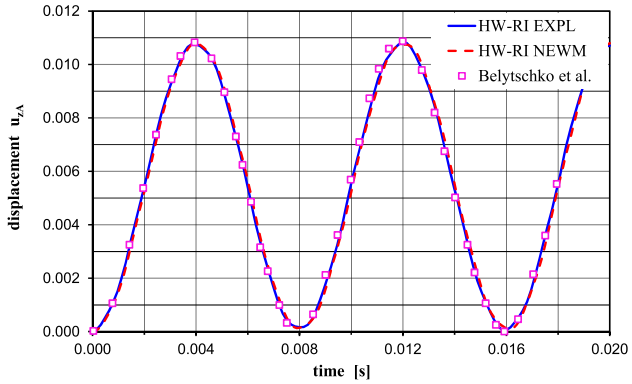

Fig. 14 Twisted beam: $u_{zA} - t$

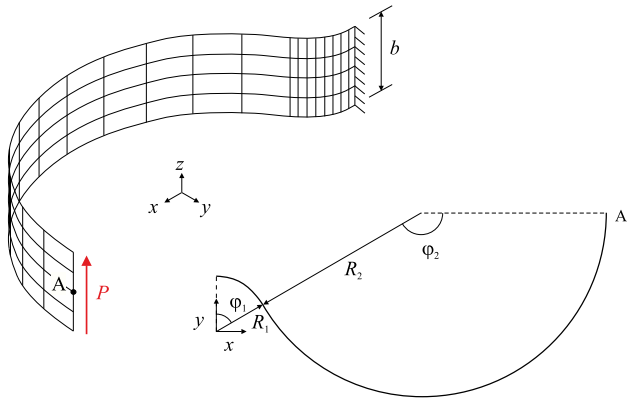

Fig. 15 Hook problem: geometry and a $4 \times 8 \times 12$ regular mesh

5.6 Hook problem

Next, we consider the hook problem shown in Fig. 15, referred to in linear analysis as the Raasch challenge, [49]. For the FE-discretization we use $N \times 2N \times 3N$ elements with N elements in width direction, $2N$ elements for the first arch (radius R_1) and $3N$ elements for the second arch (radius R_2), see Fig. 15.

Geometrical and material data are $R_1 = 14$, $\varphi_1 = 60°$, $R_2 = 46$, $\varphi_2 = 150°$, $b = 20$, thickness $h = 0.02$ and $E = 3.3 \cdot 10^3$, $\nu = 0.3$, respectively. The structure is fully clamped at one end and is loaded by a shear load P applied as a uniformly distributed traction at the free end. For the solution, we use a regular $4 \times 8 \times 12$ mesh.

Figure 16 shows the resulting load–displacement curves of point A using one point and fully integrated elements. Furthermore, curves for the MITC4+ element [34] are included. Similar results can be found for the +HW element (see Fig. 12b, 13b of Ref. [17]). The converged solutions are defined via a $32 \times 64 \times 96$ regular mesh.

A distorted mesh is shown in Fig. 17 together with a flat projection. Here, $L_{max}/L_{min} = 1.5$ is chosen for the first arch and $L_{max}/L_{min} = 2.0$ for the second arch [17].

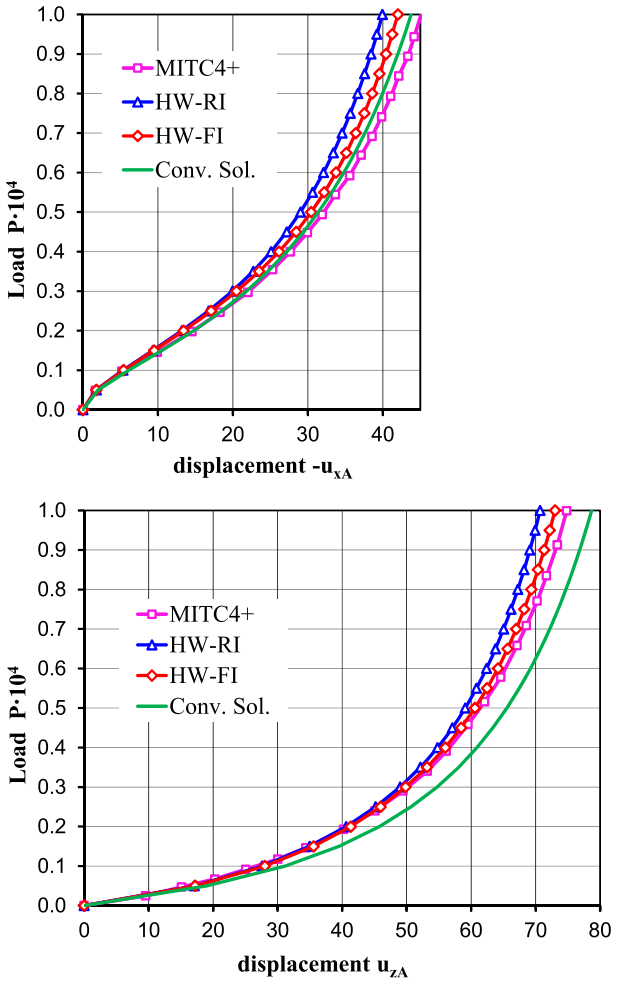

Fig. 16 Hook problem: $P - u_{xA}$ (top) and $P - u_{zA}$ (bottom) for the regular $4 \times 8 \times 12$ mesh

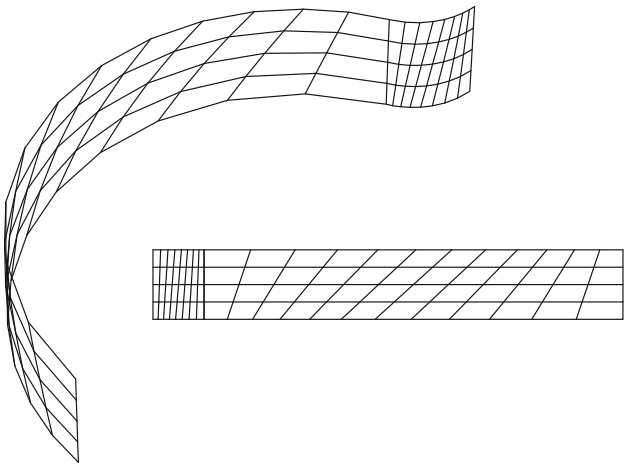

Fig. 17 Hook problem: distorted mesh and flat projection for a $4 \times 8 \times 12$ mesh

Figure 18 shows the convergence behavior of displacement u_{zA} of point A versus the number of elements N in

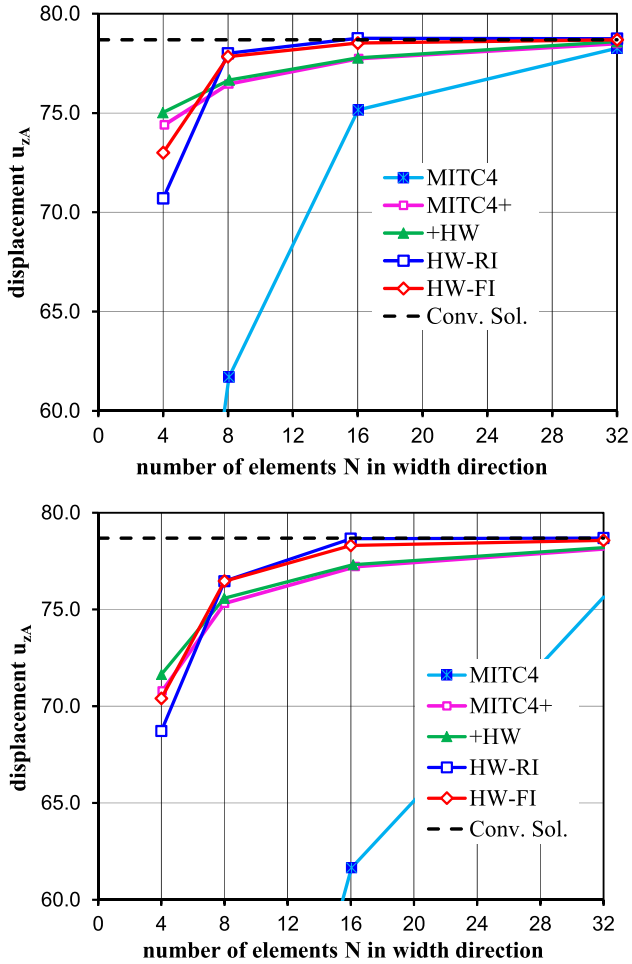

Fig. 18 Hook problem: convergence behavior $u_{zA} - N$ for regular (top) and distorted (bottom) meshes

width direction. The results for MITC4, MITC4+ and +HW are taken from Fig. 12a and 13a in Ref. [17].

A superior behavior of the MITC4+ and +HW elements as well as of present elements can be seen. The final deformed regular mesh is depicted in Fig. 19.

5.7 Channel section cantilever

This example demonstrates that present formulation is able to handle shell intersections. The channel section cantilever according to Fig. 20 is a well known test example, see for instance [50–56]. The dimensions are $L = 36\,\text{in}$, $a = 2\,\text{in}$, $b = 6\,\text{in}$, $h = 0.05\,\text{in}$, where a and b refer to the center lines of web and flange. One end of the beam is clamped, at the free end a tip load P is applied. The finite element mesh consists out of 72 elements in longitudinal direction of the beam and 8/24/8 elements in circumferential direction of the cross section. The elasticity data are $E = 10^7\,\text{lb/in}^2$ and $\nu = 0.333$, whereas plastic behavior without hardening is characterized by the yield stress

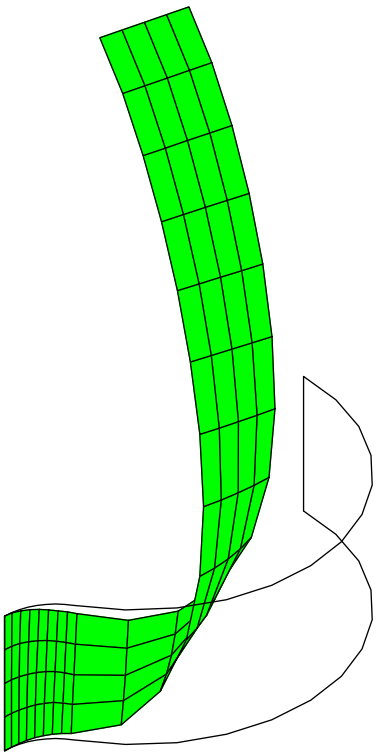

Fig. 19 Hook problem: deformed mesh for $P = 1$

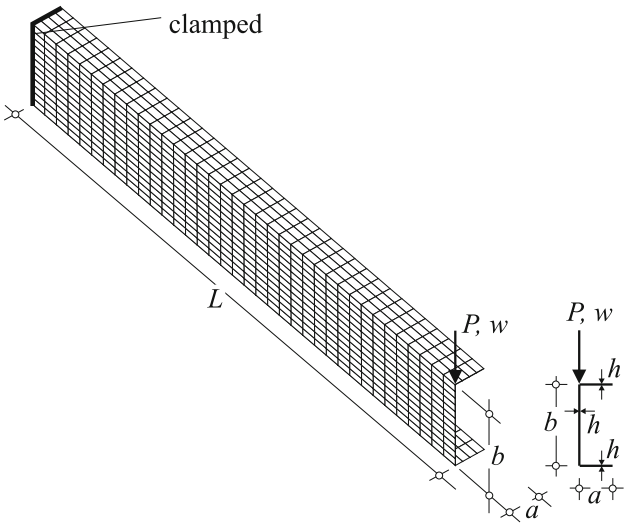

Fig. 20 Channel section cantilever with a mesh of 36×20 elements

$Y_0 = 5 \cdot 10^3$ lb/in^2. A small strain material law is used to describe the J_2-elastoplastic behavior.

The calculation is carried out applying the arc-length method, where the displacement w in direction of the load is prescribed using displacement control. The thickness integration of the stress resultants and of the material matrix is performed with four Gauss quadrature points in total. In Fig. 21 the computed load P is plotted versus the deflection

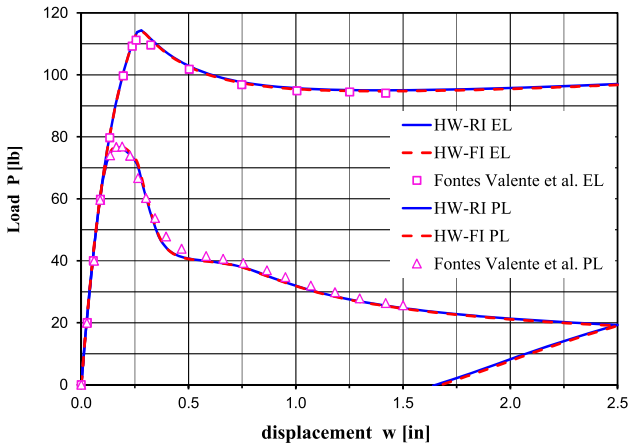

Fig. 21 Channel section cantilever: load deflection curve for the vertical displacement w

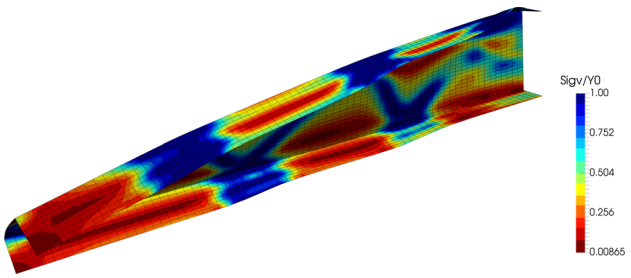

Fig. 22 Deformed configuration of the channel section cantilever at $w = 2.5$ in with a plot of the normalized von Mises stress σ_v/Y_0 of the midsurface

w for pure elastic behavior and for elasto-plastic behavior including an unloading path. Present solutions using one point quadrature agree with the results of full integration. The findings of Ref. [54] are also included. In Fig. 22 the deformed configuration at $w = 2.5$ in with a plot of the normalized von Mises stress σ_v/Y_0 at the midsurface is shown. The equivalent plastic strains are less than 2 %.

5.8 Cylindrical shell subjected to large strains

A cylindrical shell with thickness h is depicted in Fig. 23, see also [40]. The structure is clamped at $x_2 = L$ and symmetry conditions are imposed at $x_1 = 0$ and $x_3 = 0$. The shell is loaded by a concentrated force F and a distributed tension load p applied at $x_2 = 0$. In this way the structure undergoes large strains. For the reference solution using solid shell elements F is distributed as a line load $f = F/h$ and p as a surface load $q = p/h$ through the thickness. The geometrical data are summarized in Fig. 23. The material behavior is described by a Neo-Hookean strain energy

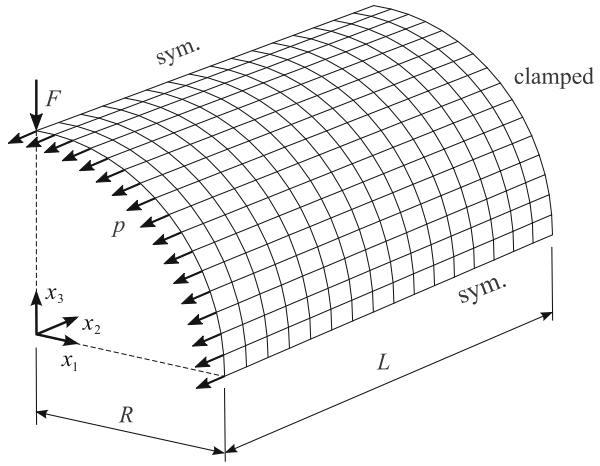

Geometrical data: $L = 300$ mm $R = 100$ mm $h = 5$ mm

Fig. 23 Cylindrical shell with a 16 × 16 mesh

$$W(\mathbf{C}) = \frac{\mu}{2}(\mathrm{tr}\,\mathbf{C} - 3 - \ln(\det \mathbf{C})) + \frac{\Lambda}{4}(\det \mathbf{C} - 1 - \ln(\det \mathbf{C}))\,. \quad (33)$$

Here, $\mathbf{C}$ is the right Cauchy-Green tensor. It is computed with the independent shell strains $\boldsymbol{\varepsilon}$, see the Hu–Washizu functional (1). The constants are chosen as $\mu = 2.1125$ N/mm^2 and $\Lambda = 1000$ N/mm^2. With $\Lambda \gg \mu$ a quasi incompressible material behavior is considered. The thickness integration of the stress resultants and of the material matrix is performed with two Gauss quadrature points in total.

Proportional loading is applied with $F = \lambda\, F_0$, $p = \lambda\, p_0$, where λ is the load factor and $F_0 = 0.25$ N as well as $p_0 = 0.1$ N/mm. The load deflection curves are computed load controlled with an increase of the load factor λ. They are shown in Figs. 24 and 25 with $u = -u_2(0, 0, R)$ as well as $w = -u_3(0, 0, R)$. With a 32×32 mesh converged solutions are obtained. There is good agreement with the 3D reference solution computed with a mesh of $64 \times 64 \times 4$ solid shell elements [57]. Furthermore, the total load can be applied with only two load steps and 12 iterations. The maximum initial step size is $\Delta\lambda = 27$. With a displacement based element or an enhanced strain element such a load step leads to divergence. Contour plots of the displacements u_3 are plotted with respect to the final deformed configuration in Fig. 26. The alternative computation of the load deflection curve with the FE2 method [40] and fully integrated shell elements (3×3 Gauss points for $n > 7$) is by a factor 8.9 longer than the computation with present one point integrated elements. This follows from the fact that for FE2 methods the computing time is dominated by the solution of the micro problems.

5.9 Square plate with spherical inclusions

The last example is computed applying the FE2 algorithm developed in [40]. We consider an inhomogeneous square plate according to Fig. 27 with constant loads $\bar{p} = \lambda \cdot 0.15 \cdot$

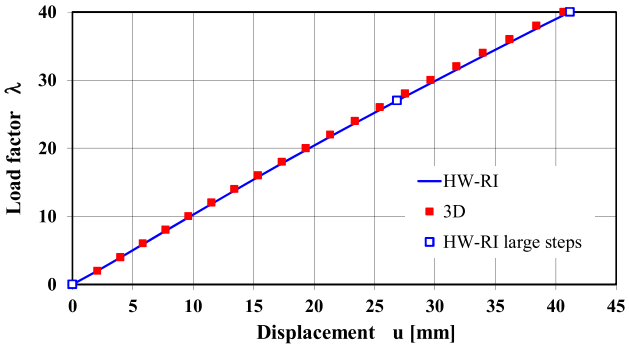

Fig. 24 Cylindrical shell: load factor λ versus displacement u

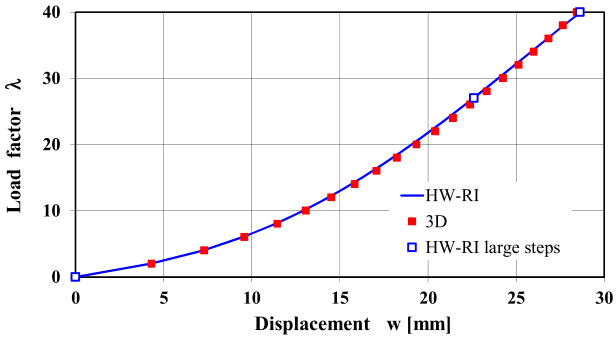

Fig. 25 Cylindrical shell: load factor λ versus displacement w

10^{-2} kN/cm^2 acting half on the upper and half on the lower surface. The span of the plate is $L = 1000$ cm and the thickness is $h = 50$ cm. It is simply supported (soft support) at all boundaries.

The plate consists of 20×20 evenly distributed unit cells with spherical inclusions, see Fig. 27. The dimensions are $l_x = l_y = h = 50$ cm and the diameter of the sphere is 35 cm. The outer material of a cell (Material 1) behaves elasto-plastic with linear isotropic hardening, whereas the soft inner material (Material 2) is linear elastic. The material data are summarized as follows:

$$\begin{aligned} \text{Material 1: } & E_1 = 3050 \text{ kN/cm}^2 \\ & \nu_1 = 0.2 \\ & Y_0 = 3.3 \text{ kN/cm}^2 \\ & \xi = 30.5 \text{ kN/cm}^2 \\ \text{Material 2: } & E_2 = 30.5 \text{ kN/cm}^2 \\ & \nu_2 = 0.2 \end{aligned} \quad (34)$$

Hereby, E_α and ν_α $(\alpha = 1, 2)$ denote the respective Young's modulus and Poisson's ratio as well as Y_0 and ξ denote the yield stress and the hardening parameter. A small strain material law is used to describe the J_2-elastoplastic behavior.

Considering symmetry one quarter of the plate is discretized with 10×10 4-node shell elements. The used representative volume element (RVE) corresponds to the unit cell depicted in Fig. 27. It is discretized with 4462 nodes and

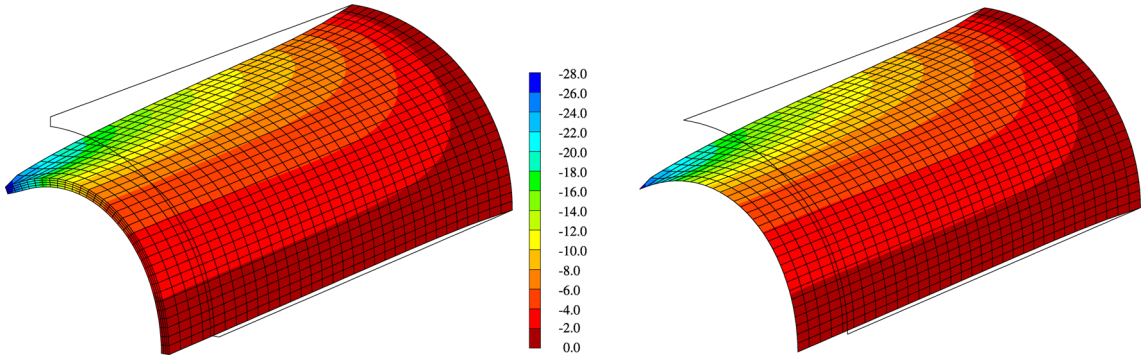

Fig. 26 Cylindrical shell: displacement u_3 [mm] (left: 3D, right: 2D HW-RI)

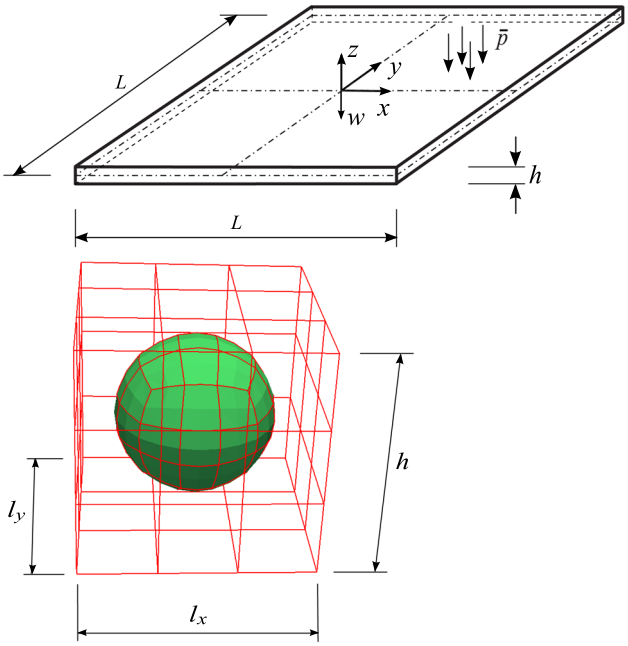

Fig. 27 Square plate with spherical inclusions and unit cell

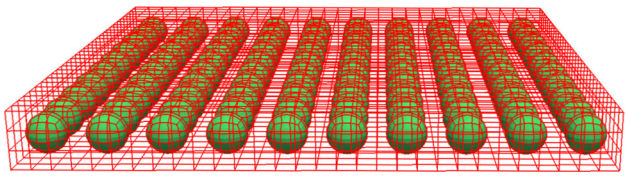

Fig. 28 3D mesh of one quarter of the plate

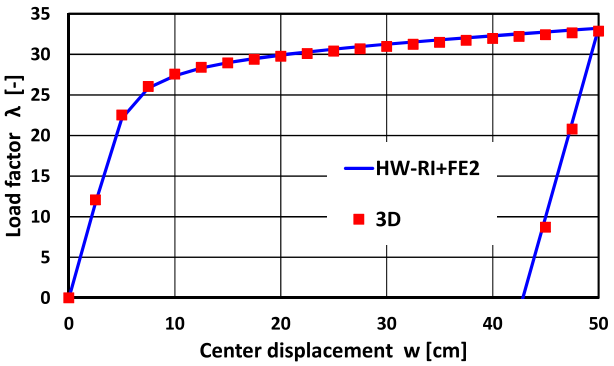

Fig. 29 Load factor λ versus displacement w

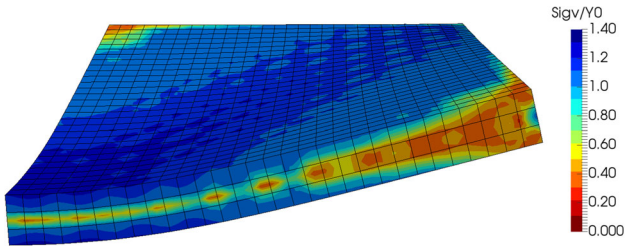

Fig. 30 One quarter of the deformed plate, normalized von Mises stresses σ_v/Y_0 (3D)

351 27-noded solid elements. Again considering symmetry conditions a full 3D discretization of one quarter of the plate is performed to compute a comparative solution. A plot of the mesh with 165862 nodes and 11200 27-noded solid elements is shown in Fig. 28.

The geometrical linear computation of the loading and unloading path is achieved applying an arclength method with displacement control and increments $\Delta w = 2.5$ cm. The computed load factors λ are plotted versus the center displacement w in Fig. 29. There is good agreement of present FE2 results with the 3D reference solution. In Fig. 30 a plot of the normalized von Mises stress σ_v/Y_0 at $w = 50$ cm is shown for one quarter of the plate. The deformed plate at $w = 50$ cm is depicted in Fig. 31. The displacements are amplified by a factor two. For present problem the computing time using a fully integrated element (2×2 integration) is by a factor 3.9 longer than that for the one point integrated element.

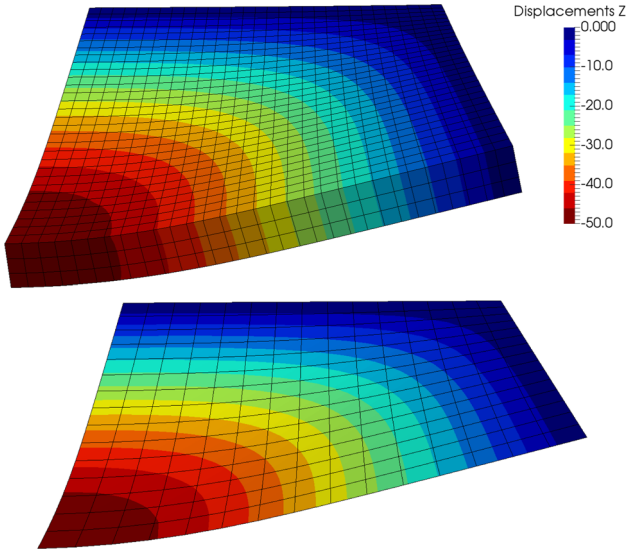

Fig. 31 One quarter of the deformed plate at $w = 50$ cm (above: 3D, below: 2D HW-RI + FE2)

6 Conclusions

The computed examples show that the new one point integrated shell element with physical hourglass stabilization shows an outstanding behavior within the scope of linear and nonlinear shell computations. The element is free of locking and reveals a high accuracy for coarse and distorted meshes. An input of problem dependent control parameters is not necessary. It can be applied to static and dynamic problems without further adaptions. Large strain problems can be accounted for. The membrane and bending patch tests are fulfilled. With 5 or 6 nodal degrees of freedoms shell problems with kinks or intersections can be incorporated. An important feature of present element formulation is the remarkable robustness in nonlinear applications. It allows very large load steps in comparison to standard element formulations based on the displacement method or enhanced strain elements. One further reason of present development is to apply the element in FE2 computations. Thereby the computing time is dominated by the solution of the micro problems at the shell integration points. Depending on the used ansatz functions for the independent shell strains the new element is approximately by a factor 4 or 9 faster than the corresponding version with full integration.

A Analytical integration of some element matrices

The area element of the shell reference surface $\mathrm{d}A = |\mathbf{X}_{,\xi} \times \mathbf{X}_{,\eta}|\,\mathrm{d}\xi\,\mathrm{d}\eta$ can be approximated in case of arbitrary warped elements by $\det \mathbf{J} \approx |\mathbf{X}_{,\xi} \times \mathbf{X}_{,\eta}|$ with $\mathbf{J}$ according to (7)

$$
\begin{aligned}
\det \mathbf{J} &= j_0 + j_1\,\xi + j_2\,\eta \\
j_0 &= (\mathbf{G}^0_\xi \cdot \mathbf{t}_1)(\mathbf{G}^0_\eta \cdot \mathbf{t}_2) - (\mathbf{G}^0_\eta \cdot \mathbf{t}_1)(\mathbf{G}^0_\xi \cdot \mathbf{t}_2) = |\mathbf{G}^0_\xi \times \mathbf{G}^0_\eta| \\
j_1 &= (\mathbf{G}^0_\xi \cdot \mathbf{t}_1)(\mathbf{G}^1 \cdot \mathbf{t}_2) - (\mathbf{G}^1 \cdot \mathbf{t}_1)(\mathbf{G}^0_\xi \cdot \mathbf{t}_2) = \mathbf{t}_3 \cdot (\mathbf{G}^0_\xi \times \mathbf{G}^1) \\
j_2 &= (\mathbf{G}^1 \cdot \mathbf{t}_1)(\mathbf{G}^0_\eta \cdot \mathbf{t}_2) - (\mathbf{G}^0_\eta \cdot \mathbf{t}_1)(\mathbf{G}^1 \cdot \mathbf{t}_2) = \mathbf{t}_3 \cdot (\mathbf{G}^1 \times \mathbf{G}^0_\eta)\,.
\end{aligned}
\tag{35}
$$

The reason for the approximation is the constant element basis system $\mathbf{t}_i$ in (7). Using (35) the constants $\bar{\xi}$ and $\bar{\eta}$ yield with the element area $A_e = 4\,j_0$

$$
\begin{aligned}
\bar{\xi} &= \frac{1}{A_e} \int_{(\Omega_e)} \xi\ \mathrm{d}A = \frac{1}{3}\frac{j_1}{j_0} \\
\bar{\eta} &= \frac{1}{A_e} \int_{(\Omega_e)} \eta\ \mathrm{d}A = \frac{1}{3}\frac{j_2}{j_0}\,.
\end{aligned}
\tag{36}
$$

Furthermore, the following integrals are computed

$$
\begin{aligned}
\check{\mathbf{I}} &= \begin{bmatrix} \check{I}_{11} & \check{I}_{12} \\ \check{I}_{21} & \check{I}_{22} \end{bmatrix} \\
&= \frac{1}{A_e} \int_{(\Omega_e)} \begin{bmatrix} (\xi - \bar{\xi})\,(\xi - \bar{\xi}) & (\xi - \bar{\xi})\,(\eta - \bar{\eta}) \\ (\eta - \bar{\eta})\,(\xi - \bar{\xi}) & (\xi - \bar{\xi})\,(\xi - \bar{\xi}) \end{bmatrix} \mathrm{d}A \\
\check{I}_{11} &= \frac{1}{3} - \bar{\eta}^2, \quad \check{I}_{22} = \frac{1}{3} - \bar{\xi}^2, \quad \check{I}_{12} = \check{I}_{21} = -\bar{\xi}\,\bar{\eta}\,.
\end{aligned}
\tag{37}
$$

One obtains the same results when $\bar{\xi}$ or $\bar{\eta}$ is omitted in one of the brackets of the integrand. This follows with Eq. (14).

The first two column vectors of $\mathbf{T}^0$ according to Eq. (9) are defined with $b = 1$ as

$$
\mathbf{i}_1 := \begin{bmatrix} J^0_{11}\,J^0_{11} \\ J^0_{12}\,J^0_{12} \\ J^0_{11}\,J^0_{12} \end{bmatrix} \qquad \mathbf{i}_2 := \begin{bmatrix} J^0_{21}\,J^0_{21} \\ J^0_{22}\,J^0_{22} \\ J^0_{21}\,J^0_{22} \end{bmatrix}. \tag{38}
$$

With these preliminary results the following matrices can be integrated analytically.

A.1 Matrix $\mathbf{F}_{22}$

The components F^{ij}_{22} of the matrix

$$
\mathbf{F}_{22} = [F^{ij}_{22}]_{6\times 6} = -\int_{\Omega_e} \mathbf{N}^{2T}_\varepsilon\,\mathbf{N}^2_\sigma\ \mathrm{d}A \tag{39}
$$

are computed via $F_{22}^{ij} = -\check{F}_{22}^{(ij)}\,\check{I}_{22}^{(ij)}$, where no summation over the indices (ij) takes place. Here, $\check{F}_{22}^{(ij)}$ are the components of

$$\check{\mathbf{F}}_{22} = \check{\mathbf{N}}_{\varepsilon}^{2T}\,\check{\mathbf{N}}_{\sigma}^{2} \qquad \check{\mathbf{N}}_{\varepsilon}^{2} = \mathbf{T}_{\varepsilon}\,\check{\mathbf{M}} \qquad \check{\mathbf{N}}_{\sigma}^{2} = \mathbf{T}_{\sigma}\,\check{\mathbf{M}}$$
$$\check{\mathbf{M}} = \begin{bmatrix} \mathbf{I}_3 & \mathbf{0} & \mathbf{0} \\ \mathbf{0} & \mathbf{I}_3 & \mathbf{0} \\ \mathbf{0} & \mathbf{0} & \mathbf{I}_2 \end{bmatrix} \qquad \mathbf{I}_3 = \begin{bmatrix} 1 & 0 \\ 0 & 1 \\ 0 & 0 \end{bmatrix} \qquad \mathbf{I}_2 = \begin{bmatrix} 1 & 0 \\ 0 & 1 \end{bmatrix} \tag{40}$$

and $\check{I}_{22}^{(ij)}$ are the components of

$$\check{\mathbf{I}}_{22} = A_e \begin{bmatrix} \check{\mathbf{I}} & \check{\mathbf{I}} & \check{\mathbf{I}} \\ \check{\mathbf{I}} & \check{\mathbf{I}} & \check{\mathbf{I}} \\ \check{\mathbf{I}} & \check{\mathbf{I}} & \check{\mathbf{I}} \end{bmatrix}_{6\times 6} \tag{41}$$

where $\check{\mathbf{I}}$ is given in (37). Due to the diagonal structure of $\check{\mathbf{F}}_{22}$ the matrix $\mathbf{F}_{22}$ possesses likewise a diagonal structure, consisting of 2×2 submatrices.

A.2 Matrix $\mathbf{H}_{22}$

The components H_{22}^{ij} of the matrix

$$\mathbf{H}_{22} = [H_{22}^{ij}]_{6\times 6} \tag{42}$$

are computed via $H_{22}^{ij} = \check{H}_{22}^{(ij)}\,\check{I}_{22}^{(ij)}$, where no summation over the indices (ij) takes place. Thereby $\check{H}_{22}^{(ij)}$ are the components of $\check{\mathbf{H}}_{22} = \check{\mathbf{N}}_{\varepsilon}^{2T}\,\mathbf{C}\,\check{\mathbf{N}}_{\varepsilon}^{2}$ with $\check{\mathbf{N}}_{\varepsilon}^{2}$ given in (40) and $\check{I}_{22}^{(ij)}$ are the components of $\check{\mathbf{I}}_{22}$ according to (41). In general $\mathbf{H}_{22}$ is fully populated.

A.3 Matrix $\mathbf{H}_{23}$

The components H_{23}^{ij} of the matrix

$$\mathbf{H}_{23} = \mathbf{H}_{32}^{T} = [H_{23}^{ij}]_{6\times n} \tag{43}$$

are computed via $H_{23}^{ij} = \check{H}_{23}^{(ij)}\,\check{I}_{23}^{(ij)}$, where no summation over the indices (ij) takes place. Thereby $\check{H}_{23}^{(ij)}$ are the components of $\check{\mathbf{H}}_{23} = \check{\mathbf{N}}_{\varepsilon}^{2T}\,\mathbf{C}\,\check{\mathbf{N}}_{\varepsilon}^{3}$ with $\check{\mathbf{N}}_{\varepsilon}^{2}$ according to (40) and $\check{I}_{23}^{(ij)}$ are the components of matrix $\check{\mathbf{I}}_{23}$. It holds

$$\check{\mathbf{N}}_{\varepsilon}^{3} = \mathbf{T}_{\varepsilon}\,\check{\mathbf{M}}_{\varepsilon}^{3}$$
$$\check{\mathbf{M}}_{\varepsilon}^{3} = \begin{bmatrix} \check{\mathbf{M}}_{\varepsilon m}^{3} \\ \mathbf{0} \\ \mathbf{0} \end{bmatrix}_{8\times n}$$
$$\check{\mathbf{M}}_{\varepsilon m}^{3} = \begin{bmatrix} 1&0&0&0&1&0&0&1&0&1&0&0&0 \\ 0&1&0&0&0&1&0&0&1&0&1&0&0 \\ 0&0&1&1&0&0&1&0&0&0&0&1&1 \end{bmatrix}$$
$$\check{\mathbf{I}}_{23} = A_e \begin{bmatrix} \hat{\mathbf{I}} \\ \hat{\mathbf{I}} \\ \hat{\mathbf{I}} \end{bmatrix}$$
$$\hat{\mathbf{I}} = \begin{bmatrix} \check{I}_{12} & \check{I}_{11} & \check{I}_{12} & \check{I}_{11} & \frac{1}{3}\bar{\xi} & \frac{1}{3}\bar{\xi} & \frac{1}{3}\bar{\xi} & \bar{I}_{11} & \bar{I}_{21} & \bar{I}_{21} & \bar{I}_{11} & \bar{I}_{11} & \bar{I}_{21} \\ \check{I}_{22} & \check{I}_{21} & \check{I}_{22} & \check{I}_{12} & \frac{1}{3}\bar{\eta} & \frac{1}{3}\bar{\eta} & \frac{1}{3}\bar{\eta} & \bar{I}_{12} & \bar{I}_{22} & \bar{I}_{22} & \bar{I}_{21} & \bar{I}_{12} & \bar{I}_{22} \end{bmatrix} \tag{44}$$

where the integrals $\check{I}_{\alpha\beta}$ $\alpha, \beta = 1, 2$ are computed in (37) and $\bar{I}_{\alpha\beta} = (\frac{1}{3} - c)\,\check{I}_{\alpha\beta}$. In general $\mathbf{H}_{23}$ is fully populated.

A.4 Matrix $\mathbf{H}_{33}$

The components H_{33}^{ij} of the matrix

$$\mathbf{H}_{33} = [H_{33}^{ij}]_{n\times n} \tag{45}$$

are computed via $H_{33}^{ij} = \check{H}_{33}^{(ij)}\,\check{I}_{33}^{(ij)}$, where no summation over the indices (ij) takes place. Thereby $\check{H}_{33}^{(ij)}$ are the components of $\check{\mathbf{H}}_{33} = \check{\mathbf{N}}_{\varepsilon}^{3T}\,\mathbf{C}\,\check{\mathbf{N}}_{\varepsilon}^{3}$ with $\check{\mathbf{N}}_{\varepsilon}^{3}$ according to (44) and $\check{I}_{33}^{(ij)}$ are the components of $\check{\mathbf{I}}_{33}$. It holds

$$\check{\mathbf{I}}_{33} = A_e \begin{bmatrix}
\frac{1}{3} & & & & & & & & \\
0 & \frac{1}{3} & & & & & & & \\
\frac{1}{3} & 0 & \frac{1}{3} & & & & & & \\
0 & \frac{1}{3} & 0 & \frac{1}{3} & & & & \text{sym.} & \\
\frac{1}{3}\bar{\eta} & \frac{1}{3}\bar{\xi} & \frac{1}{3}\bar{\eta} & \frac{1}{3}\bar{\xi} & \frac{1}{9} & & & & \\
\frac{1}{3}\bar{\eta} & \frac{1}{3}\bar{\xi} & \frac{1}{3}\bar{\eta} & \frac{1}{3}\bar{\xi} & \frac{1}{9} & \frac{1}{9} & & & \\
\frac{1}{3}\bar{\eta} & \frac{1}{3}\bar{\xi} & \frac{1}{3}\bar{\eta} & \frac{1}{3}\bar{\xi} & \frac{1}{9} & \frac{1}{9} & \frac{1}{9} & & \\
0 & c_1 & 0 & c_1 & c_2 & c_2 & c_2 & c_4 & \\
c_1 & 0 & c_1 & 0 & c_3 & c_3 & c_3 & 0 & c_4 \\
c_1 & 0 & c_1 & 0 & c_3 & c_3 & c_3 & 0 & c_4 & c_4 \\
0 & c_1 & 0 & c_1 & c_2 & c_2 & c_2 & c_4 & 0 & 0 & c_4 \\
0 & c_1 & 0 & c_1 & c_2 & c_2 & c_2 & c_4 & 0 & 0 & c_4 & c_4 \\
c_1 & 0 & c_1 & 0 & c_3 & c_3 & c_3 & 0 & c_4 & c_4 & 0 & 0 & c_4
\end{bmatrix}, \tag{46}$$

where

$$c_1 = \tfrac{1}{9} - \tfrac{1}{3}\,c \;, c_2 = (\tfrac{1}{5} - \tfrac{1}{3}\,c)\,\bar{\xi} \;,$$

$$c_3 = (\tfrac{1}{5} - \tfrac{1}{3}\,c)\,\bar{\eta}\ ,\ c_4 = \tfrac{1}{3}\,(\tfrac{1}{5} - \tfrac{2}{3}\,c + c^2).$$

A.5 Vector $\mathbf{f}_{21}^s$

To allow for an analytical integration of $\mathbf{f}_{21}^s := \int_{\Omega_e} \mathbf{N}_\sigma^{2T}\,\boldsymbol{\varepsilon}_g^h\,\mathrm{d}A$ a series expansion of the geometrical membrane strains and curvatures in $\boldsymbol{\varepsilon}_g^h = [\boldsymbol{\varepsilon}_m, \boldsymbol{\varepsilon}_b, \boldsymbol{\varepsilon}_s]^T$ at $\xi = \eta = 0$ is performed up to linear terms in ξ and η:

$$\begin{aligned}
\boldsymbol{\varepsilon}_m &= \boldsymbol{\varepsilon}_{m0} + \boldsymbol{\varepsilon}_m^\xi\,\xi + \boldsymbol{\varepsilon}_m^\eta\,\eta \\
\boldsymbol{\varepsilon}_{m0} &:= \boldsymbol{\varepsilon}_m(\xi = \eta = 0)\,, \quad \boldsymbol{\varepsilon}_m^\xi := \partial_\xi \boldsymbol{\varepsilon}_m\,, \quad \boldsymbol{\varepsilon}_m^\eta := \partial_\eta \boldsymbol{\varepsilon}_m \\
\boldsymbol{\varepsilon}_b &= \boldsymbol{\varepsilon}_{b0} + \boldsymbol{\varepsilon}_b^\xi\,\xi + \boldsymbol{\varepsilon}_b^\eta\,\eta \\
\boldsymbol{\varepsilon}_{b0} &:= \boldsymbol{\varepsilon}_b(\xi = \eta = 0)\,, \quad \boldsymbol{\varepsilon}_b^\xi := \partial_\xi \boldsymbol{\varepsilon}_b\,, \quad \boldsymbol{\varepsilon}_b^\eta := \partial_\eta \boldsymbol{\varepsilon}_b\,.
\end{aligned} \tag{47}$$

Application of the chain rule yields

$$\begin{aligned}
\boldsymbol{\varepsilon}_m^\xi &= J_{11}^0\,\boldsymbol{\varepsilon}_m^1 + J_{12}^0\,\boldsymbol{\varepsilon}_m^2 \\
\boldsymbol{\varepsilon}_m^\eta &= J_{21}^0\,\boldsymbol{\varepsilon}_m^1 + J_{22}^0\,\boldsymbol{\varepsilon}_m^2 \\
\boldsymbol{\varepsilon}_b^\xi &= J_{11}^0\,\boldsymbol{\varepsilon}_b^1 + J_{12}^0\,\boldsymbol{\varepsilon}_b^2 \\
\boldsymbol{\varepsilon}_b^\eta &= J_{21}^0\,\boldsymbol{\varepsilon}_b^1 + J_{22}^0\,\boldsymbol{\varepsilon}_b^2
\end{aligned} \tag{48}$$

with

$$\boldsymbol{\varepsilon}_m^1 = \begin{bmatrix} \mathbf{x}_{,11}\cdot\mathbf{x}_{,1} - \mathbf{X}_{,11}\cdot\mathbf{X}_{,1} \\ \mathbf{x}_{,21}\cdot\mathbf{x}_{,2} - \mathbf{X}_{,21}\cdot\mathbf{X}_{,2} \\ \mathbf{x}_{,11}\cdot\mathbf{x}_{,2} + \mathbf{x}_{,21}\cdot\mathbf{x}_{,1} - \mathbf{X}_{,11}\cdot\mathbf{X}_{,2} - \mathbf{X}_{,21}\cdot\mathbf{X}_{,1} \end{bmatrix}$$

$$\boldsymbol{\varepsilon}_m^2 = \begin{bmatrix} \mathbf{x}_{,12}\cdot\mathbf{x}_{,1} - \mathbf{X}_{,12}\cdot\mathbf{X}_{,1} \\ \mathbf{x}_{,22}\cdot\mathbf{x}_{,2} - \mathbf{X}_{,22}\cdot\mathbf{X}_{,2} \\ \mathbf{x}_{,12}\cdot\mathbf{x}_{,2} + \mathbf{x}_{,22}\cdot\mathbf{x}_{,1} - \mathbf{X}_{,12}\cdot\mathbf{X}_{,2} - \mathbf{X}_{,22}\cdot\mathbf{X}_{,1} \end{bmatrix}$$

$$\boldsymbol{\varepsilon}_b^1 = \begin{bmatrix} \mathbf{x}_{,11}\cdot\mathbf{d}_{,1} + \mathbf{d}_{,11}\cdot\mathbf{x}_{,1} - \mathbf{X}_{,11}\cdot\mathbf{D}_{,1} - \mathbf{D}_{,11}\cdot\mathbf{X}_{,1} \\ \mathbf{x}_{,21}\cdot\mathbf{d}_{,2} + \mathbf{d}_{,21}\cdot\mathbf{x}_{,2} - \mathbf{X}_{,21}\cdot\mathbf{D}_{,2} - \mathbf{D}_{,21}\cdot\mathbf{X}_{,2} \\ \mathbf{x}_{,11}\cdot\mathbf{d}_{,2} + \mathbf{d}_{,21}\cdot\mathbf{x}_{,1} + \mathbf{x}_{,21}\cdot\mathbf{d}_{,1} + \mathbf{d}_{,11}\cdot\mathbf{x}_{,2} \\ -\mathbf{X}_{,11}\cdot\mathbf{D}_{,2} - \mathbf{D}_{,21}\cdot\mathbf{X}_{,1} - \mathbf{X}_{,21}\cdot\mathbf{D}_{,1} - \mathbf{D}_{,11}\cdot\mathbf{X}_{,2} \end{bmatrix}$$

$$\boldsymbol{\varepsilon}_b^2 = \begin{bmatrix} \mathbf{x}_{,12}\cdot\mathbf{d}_{,1} + \mathbf{d}_{,12}\cdot\mathbf{x}_{,1} - \mathbf{X}_{,12}\cdot\mathbf{D}_{,1} - \mathbf{D}_{,12}\cdot\mathbf{X}_{,1} \\ \mathbf{x}_{,22}\cdot\mathbf{d}_{,2} + \mathbf{d}_{,22}\cdot\mathbf{x}_{,2} - \mathbf{X}_{,22}\cdot\mathbf{D}_{,2} - \mathbf{D}_{,22}\cdot\mathbf{X}_{,2} \\ \mathbf{x}_{,12}\cdot\mathbf{d}_{,2} + \mathbf{d}_{,22}\cdot\mathbf{x}_{,1} + \mathbf{x}_{,22}\cdot\mathbf{d}_{,1} + \mathbf{d}_{,12}\cdot\mathbf{x}_{,2} \\ -\mathbf{X}_{,12}\cdot\mathbf{D}_{,2} - \mathbf{D}_{,22}\cdot\mathbf{X}_{,1} - \mathbf{X}_{,22}\cdot\mathbf{D}_{,1} - \mathbf{D}_{,12}\cdot\mathbf{X}_{,2} \end{bmatrix}. \tag{49}$$

In case of a geometrical linear shell element the expressions in (49) have to be replaced by the corresponding terms of the linear shell theory. The vectors $\mathbf{x}_{,\alpha\beta}$ and $\mathbf{d}_{,\alpha\beta}$ are obtained with

$$\begin{aligned}
\mathbf{x}_{,\alpha\beta} &= \sum_{I=1}^{4} N_{I,\alpha\beta}\ (\mathbf{X}_I + \mathbf{u}_I) \qquad \alpha, \beta = 1, 2 \\
\mathbf{d}_{,\alpha\beta} &= \sum_{I=1}^{4} N_{I,\alpha\beta}\ \mathbf{d}_I
\end{aligned} \tag{50}$$

and in analogues way for $\mathbf{X}_{,\alpha\beta}$ and $\mathbf{D}_{,\alpha\beta}$. Concerning the second derivatives of the shape functions N_I we refer to the representation in Ref. [58]. Note, that $\boldsymbol{\varepsilon}_{m0}$ and $\boldsymbol{\varepsilon}_{b0}$ do not depend on ξ and η and thus can be taken out of the integral. For this reason they do not contribute to $\mathbf{f}_{21}^s$ taking Eqs. (13) and (14) into account. The series expansion is not necessary for the transverse shear strains $\boldsymbol{\varepsilon}_s$. This follows from the assumed strain interpolation in (10) which directly leads to positive whole-number powers of ξ and η in the integrand of $\mathbf{f}_{21}^s$.

Considering (47–50) the integration can now be performed. One obtains

$$\mathbf{f}_{21}^s = A_e \begin{bmatrix} \mathbf{i}_1\cdot(\check{I}_{11}\,\boldsymbol{\varepsilon}_m^\eta + \check{I}_{12}\,\boldsymbol{\varepsilon}_m^\xi) \\ \mathbf{i}_2\cdot(\check{I}_{21}\,\boldsymbol{\varepsilon}_m^\eta + \check{I}_{22}\,\boldsymbol{\varepsilon}_m^\xi) \\ \mathbf{i}_1\cdot(\check{I}_{11}\,\boldsymbol{\varepsilon}_b^\eta + \check{I}_{12}\,\boldsymbol{\varepsilon}_b^\xi) \\ \mathbf{i}_2\cdot(\check{I}_{21}\,\boldsymbol{\varepsilon}_b^\eta + \check{I}_{22}\,\boldsymbol{\varepsilon}_b^\xi) \\ \frac{1}{2}\,[\frac{1}{3}(\gamma_\xi^D - \gamma_\xi^B) - \bar{\xi}\,(\gamma_\eta^C + \gamma_\eta^A) - \bar{\eta}\,(\gamma_\xi^D + \gamma_\xi^B)] \\ \frac{1}{2}\,[\frac{1}{3}(\gamma_\eta^C - \gamma_\eta^A) - \bar{\xi}\,(\gamma_\eta^C + \gamma_\eta^A) - \bar{\eta}\,(\gamma_\xi^D + \gamma_\xi^B)] \end{bmatrix}, \tag{51}$$

where $\gamma_\eta^A, \gamma_\xi^B, \gamma_\eta^C, \gamma_\xi^D$ are specified in [11]. The integrals $\check{I}_{\alpha\beta}$ have been computed in (37) and the vectors $\mathbf{i}_1, \mathbf{i}_2$ are defined in (38).

A.6 Matrix $\mathbf{G}_2$

Let $\mathbf{B}_I$ and $\mathbf{G}_{2I}$ be the submatrices of $\mathbf{B}$ and $\mathbf{G}_2 = \int_{\Omega_e} \mathbf{N}_\sigma^{2T}\,\mathbf{B}\,\mathrm{d}A$ related to node $I \in \{1, 2, 3, 4\}$, respectively. The submatrices of $\mathbf{B}_I$ for membrane, bending and shear

$$\mathbf{B}_I = \begin{bmatrix} \mathbf{B}_{mI} & \mathbf{0} \\ \mathbf{B}_{bI} & \mathbf{B}_{mI}\mathbf{T}_I \\ \mathbf{B}_{suI} & \mathbf{B}_{s\beta I} \end{bmatrix} \tag{52}$$

are explicitly specified in [11]. To allow for an analytical integration of $\mathbf{G}_{2I}$ the series expansion of $\mathbf{B}_{mI}$ and $\mathbf{B}_{bI}$ at $\xi = \eta = 0$ is performed up to linear terms in ξ and η:

$$\begin{aligned}
\mathbf{B}_{mI} &= \mathbf{B}_{mI0} + \mathbf{B}_{mI}^\xi\,\xi + \mathbf{B}_{mI}^\eta\,\eta \\
\mathbf{B}_{mI0} &:= \mathbf{B}_{mI}(\xi = \eta = 0)\,, \ \mathbf{B}_{mI}^\xi := \partial_\xi \mathbf{B}_{mI}\,, \ \mathbf{B}_{mI}^\eta := \partial_\eta \mathbf{B}_{mI} \\
\mathbf{B}_{bI} &= \mathbf{B}_{bI0} + \mathbf{B}_{bI}^\xi\,\xi + \mathbf{B}_{bI}^\eta\,\eta \\
\mathbf{B}_{bI0} &:= \mathbf{B}_{bI}(\xi = \eta = 0)\,, \ \mathbf{B}_{bI}^\xi := \partial_\xi \mathbf{B}_{bI}\,, \ \mathbf{B}_{bI}^\eta := \partial_\eta \mathbf{B}_{bI}\,.
\end{aligned} \tag{53}$$

Application of the chain rule yields

$$\begin{aligned}
\mathbf{B}^{\xi}_{mI} &= J^0_{11}\,\mathbf{B}^1_{mI} + J^0_{12}\,\mathbf{B}^2_{mI}\\
\mathbf{B}^{\eta}_{mI} &= J^0_{21}\,\mathbf{B}^1_{mI} + J^0_{22}\,\mathbf{B}^2_{mI}\\
\mathbf{B}^{\xi}_{bI} &= J^0_{11}\,\mathbf{B}^1_{bI} + J^0_{12}\,\mathbf{B}^2_{bI}\\
\mathbf{B}^{\eta}_{bI} &= J^0_{21}\,\mathbf{B}^1_{bI} + J^0_{22}\,\mathbf{B}^2_{bI}
\end{aligned} \tag{54}$$

with

$$\mathbf{B}^1_{mI} = \begin{bmatrix} N_{I,11}\,\mathbf{x}^T_{,1} + N_{I,1}\,\mathbf{x}^T_{,11} \\ N_{I,21}\,\mathbf{x}^T_{,2} + N_{I,2}\,\mathbf{x}^T_{,21} \\ N_{I,11}\,\mathbf{x}^T_{,2} + N_{I,21}\,\mathbf{x}^T_{,1} + N_{I,2}\,\mathbf{x}^T_{,11} + N_{I,1}\,\mathbf{x}^T_{,21} \end{bmatrix}$$

$$\mathbf{B}^2_{mI} = \begin{bmatrix} N_{I,12}\,\mathbf{x}^T_{,1} + N_{I,1}\,\mathbf{x}^T_{,12} \\ N_{I,22}\,\mathbf{x}^T_{,2} + N_{I,2}\,\mathbf{x}^T_{,22} \\ N_{I,12}\,\mathbf{x}^T_{,2} + N_{I,22}\,\mathbf{x}^T_{,1} + N_{I,1}\,\mathbf{x}^T_{,22} + N_{I,2}\,\mathbf{x}^T_{,12} \end{bmatrix}$$

$$\mathbf{B}^1_{bI} = \begin{bmatrix} N_{I,11}\,\mathbf{d}^T_{,1} + N_{I,1}\,\mathbf{d}^T_{,11} \\ N_{I,21}\,\mathbf{d}^T_{,2} + N_{I,2}\,\mathbf{d}^T_{,21} \\ N_{I,11}\,\mathbf{d}^T_{,2} + N_{I,21}\,\mathbf{d}^T_{,1} + N_{I,2}\,\mathbf{d}^T_{,11} + N_{I,1}\,\mathbf{d}^T_{,21} \end{bmatrix}$$

$$\mathbf{B}^2_{bI} = \begin{bmatrix} N_{I,12}\,\mathbf{d}^T_{,1} + N_{I,1}\,\mathbf{d}^T_{,12} \\ N_{I,22}\,\mathbf{d}^T_{,2} + N_{I,2}\,\mathbf{d}^T_{,22} \\ N_{I,12}\,\mathbf{d}^T_{,2} + N_{I,22}\,\mathbf{d}^T_{,1} + N_{I,1}\,\mathbf{d}^T_{,22} + N_{I,2}\,\mathbf{d}^T_{,12} \end{bmatrix}. \tag{55}$$

Note, that $\mathbf{B}_{mI0}$ and $\mathbf{B}_{bI0}$ do not depend on ξ and η and thus do not contribute to $\mathbf{G}_{2I}$ considering Eqs. (13) and (14). Due to the assumed interpolation for the transverse shear strains [4] the series expansion is not necessary for $\mathbf{B}_{suI}$ and $\mathbf{B}_{s\beta I}$.

Hence, one obtains

$$\begin{aligned}
\mathbf{G}_{2I} &= A_e \begin{bmatrix} \mathbf{G}_{muI} & \mathbf{0} \\ \mathbf{G}_{buI} & \mathbf{G}_{b\beta I} \\ \mathbf{G}_{suI} & \mathbf{G}_{s\beta I} \end{bmatrix}_{6\times \mathrm{ndf}}\\
\mathbf{G}_{b\beta I} &= \mathbf{G}_{muI}\,\mathbf{T}_I\\
\mathbf{G}_{muI} &= \begin{bmatrix} \mathbf{i}^T_1 (\check{I}_{11}\,\mathbf{B}^{\eta}_{mI} + \check{I}_{12}\,\mathbf{B}^{\xi}_{mI}) \\ \mathbf{i}^T_2 (\check{I}_{21}\,\mathbf{B}^{\eta}_{mI} + \check{I}_{22}\,\mathbf{B}^{\xi}_{mI}) \end{bmatrix} = \begin{bmatrix} \check{\mathbf{g}}_{1I} \\ \check{\mathbf{g}}_{2I} \end{bmatrix}\\
\mathbf{G}_{buI} &= \begin{bmatrix} \mathbf{i}^T_1 (\check{I}_{11}\,\mathbf{B}^{\eta}_{bI} + \check{I}_{12}\,\mathbf{B}^{\xi}_{bI}) \\ \mathbf{i}^T_2 (\check{I}_{21}\,\mathbf{B}^{\eta}_{bI} + \check{I}_{22}\,\mathbf{B}^{\xi}_{bI}) \end{bmatrix}\\
\mathbf{G}_{suI} &= \begin{bmatrix} \widehat{\xi}_I\,\mathbf{d}^T_M - \frac{1}{4}\,\bar{\xi}\,\eta_I\,\mathbf{d}^T_L \\ \widehat{\eta}_I\,\mathbf{d}^T_L - \frac{1}{4}\,\bar{\eta}\,\xi_I\,\mathbf{d}^T_M \end{bmatrix}\\
\mathbf{G}_{s\beta I} &= \begin{bmatrix} \check{\eta}_I\,\mathbf{b}^T_M - \frac{1}{4}\,\bar{\xi}\,\mathbf{b}^T_L \\ \check{\xi}_I\,\mathbf{b}^T_L - \frac{1}{4}\,\bar{\eta}\,\mathbf{b}^T_M \end{bmatrix}
\end{aligned} \tag{56}$$

with $\widehat{\xi}_I = \frac{1}{4}\,\xi_I\,(\frac{1}{3}\,\eta_I - \bar{\eta})$, $\widehat{\eta}_I = \frac{1}{4}\,\eta_I\,(\frac{1}{3}\,\xi_I - \bar{\xi})$, $\check{\xi}_I = \frac{1}{4}\,(\frac{1}{3}\,\xi_I - \bar{\xi})$ and $\check{\eta}_I = \frac{1}{4}\,(\frac{1}{3}\,\eta_I - \bar{\eta})$. The integrals $\check{I}_{\alpha\beta}$ and the vectors $\mathbf{i}_1, \mathbf{i}_2$ are defined in (37) and (38), respectively. Furthermore, $\mathbf{d}_M, \mathbf{d}_L, \mathbf{b}_M, \mathbf{b}_L$ are specified in [11].

A.7 Matrix $\mathbf{K}_{g2}$

Let $\mathbf{K}_{IK}$ be the submatrix of $\mathbf{K}_{g2} = \int_{\Omega_e} \mathbf{K}_\sigma(\boldsymbol{\sigma}^h)\,\mathrm{d}A$ with $\boldsymbol{\sigma}^h = \mathbf{N}^2_\sigma\,\hat{\boldsymbol{\sigma}}_2$ related to nodes $I, K \in \{1,2,3,4\}$. To allow for an analytical integration the series expansion of

$$\mathbf{N}_{IK} := \begin{bmatrix} N_{I,1}\,N_{K,1} \\ N_{I,2}\,N_{K,2} \\ N_{I,1}\,N_{K,2} + N_{I,2}\,N_{K,1} \end{bmatrix} \tag{57}$$

at $\xi = \eta = 0$ is expressed up to linear terms in ξ and η

$$\begin{aligned}
\mathbf{N}_{IK} &= \mathbf{N}_{IK0} + \mathbf{N}^{\xi}_{IK}\,\xi + + \mathbf{N}^{\eta}_{IK}\,\eta\\
\mathbf{N}_{IK0} &:= \mathbf{N}_{IK}(\xi = \eta = 0) \quad \mathbf{N}^{\xi}_{IK} := \partial_\xi \mathbf{N}_{IK} \quad \mathbf{N}^{\eta}_{IK} := \partial_\eta \mathbf{N}_{IK}\,.
\end{aligned} \tag{58}$$

The vector $\mathbf{N}_{IK0}$ does not depend on ξ and η and therefore does not contribute to $\mathbf{K}_{IK}$ taking Eqs. (13) and (14) into account. Application of the chain rule yields

$$\begin{aligned}
\mathbf{N}^{\xi}_{IK} &= J^0_{11}\,\mathbf{N}^1_{IK} + J^0_{12}\,\mathbf{N}^2_{IK}\\
\mathbf{N}^{\eta}_{IK} &= J^0_{21}\,\mathbf{N}^1_{IK} + J^0_{22}\,\mathbf{N}^2_{IK}
\end{aligned} \tag{59}$$

with

$$\mathbf{N}^1_{IK} = \begin{bmatrix} N_{I,11}\;\; N_{K,1} + N_{K,11}\;\; N_{I,1} \\ N_{I,21}\;\; N_{K,2} + N_{K,21}\;\; N_{I,2} \\ N_{I,11}\;\; N_{K,2} + N_{K,21}\;\; N_{I,1} + N_{I,21}\;\; N_{K,1} + N_{K,11}\;\; N_{I,2} \end{bmatrix}$$

$$\mathbf{N}^2_{IK} = \begin{bmatrix} N_{I,12}\;\; N_{K,1} + N_{K,12}\;\; N_{I,1} \\ N_{I,22}\;\; N_{K,2} + N_{K,22}\;\; N_{I,2} \\ N_{I,12}\;\; N_{K,2} + N_{K,22}\;\; N_{I,1} + N_{I,22}\;\; N_{K,1} + N_{K,12}\;\; N_{I,2} \end{bmatrix}. \tag{60}$$

Hence, one obtains

$$\begin{aligned}
\mathbf{K}_{IK} &= A_e \begin{bmatrix} \hat{n}_{IK}\,\mathbf{1}_3 & (\hat{m}_{IK} + \hat{q}^{\beta u}_{IK})\mathbf{T}_K \\ (\hat{m}_{IK} + \hat{q}^{\beta u}_{IK})\mathbf{T}^T_I & \delta_{IK}\,\hat{\mathbf{M}}_I(\mathbf{h}_I) \end{bmatrix}_{\mathrm{ndf}\times\mathrm{ndf}}\\
\hat{n}_{IK} &= \mathbf{i}_1 \cdot (\check{I}_{11}\mathbf{N}^{\eta}_{IK} + \check{I}_{12}\mathbf{N}^{\xi}_{IK})\,\hat{\sigma}_9 + \mathbf{i}_2 \cdot (\check{I}_{21}\mathbf{N}^{\eta}_{IK} + \check{I}_{22}\mathbf{N}^{\xi}_{IK})\,\hat{\sigma}_{10}\\
\hat{m}_{IK} &= \mathbf{i}_1 \cdot (\check{I}_{11}\mathbf{N}^{\eta}_{IK} + \check{I}_{12}\mathbf{N}^{\xi}_{IK})\,\hat{\sigma}_{11} + \mathbf{i}_2 \cdot (\check{I}_{21}\mathbf{N}^{\eta}_{IK} + \check{I}_{22}\mathbf{N}^{\xi}_{IK})\,\hat{\sigma}_{12}\\
\hat{q}^{u\beta}_{IK} &= \tfrac{1}{2}[(\widehat{\xi}_I\,f^1_{IK} - \tfrac{1}{4}\,\bar{\xi}\,\eta_I\,f^2_{IK})\,\hat{\sigma}_{13} + (\widehat{\eta}_I\,f^2_{IK} - \tfrac{1}{4}\,\bar{\eta}\,\xi_I\,f^1_{IK})\,\hat{\sigma}_{14}]\\
\hat{q}^{\beta u}_{IK} &= \tfrac{1}{2}[(\widehat{\xi}_K\,f^1_{IK} - \tfrac{1}{4}\,\bar{\xi}\,\eta_K\,f^2_{IK})\,\hat{\sigma}_{13} + (\widehat{\eta}_K\,f^2_{IK} - \tfrac{1}{4}\,\bar{\eta}\,\xi_K\,f^1_{IK})\,\hat{\sigma}_{14}]\\
\mathbf{h}_I &= \hat{\sigma}_{11}\,\check{\mathbf{g}}_{1I} + \hat{\sigma}_{12}\,\check{\mathbf{g}}_{2I}\\
&\quad + \hat{\sigma}_{13}\,(\check{\eta}_I\,\mathbf{x}^M_{,\xi} - \tfrac{1}{4}\,\bar{\xi}\,\mathbf{x}^L_{,\eta}) + \hat{\sigma}_{14}\,(\check{\xi}_I\,\mathbf{x}^L_{,\eta} - \tfrac{1}{4}\,\bar{\eta}\,\mathbf{x}^M_{,\xi})
\end{aligned} \tag{61}$$

with

$$\widehat{\xi}_I = \tfrac{1}{4}\,\xi_I\,(\tfrac{1}{3}\,\eta_I - \bar{\eta}), \quad \widehat{\eta}_I = \tfrac{1}{4}\,\eta_I\,(\tfrac{1}{3}\,\xi_I - \bar{\xi}),$$
$$\check{\xi}_I = \tfrac{1}{4}\,(\tfrac{1}{3}\,\xi_I - \bar{\xi}), \quad \check{\eta}_I = \tfrac{1}{4}\,(\tfrac{1}{3}\,\eta_I - \bar{\eta})$$

and the corresponding expressions with index K. The quantities $\hat{\sigma}_{ij}$ are components of the parameter vector

$$\hat{\boldsymbol{\sigma}}_2 = [\hat{\sigma}_9, \hat{\sigma}_{10}, \hat{\sigma}_{11}, \hat{\sigma}_{12}, \hat{\sigma}_{13}, \hat{\sigma}_{14}]^T.$$

The integrals $\check{I}_{\alpha\beta}$ are computed in (37) and the vectors $\mathbf{i}_1, \mathbf{i}_2$, $\check{\mathbf{g}}_{1I}, \check{\mathbf{g}}_{2I}$ are defined in (38), (56) respectively. The factors f^1_{IK}, f^2_{IK}, the vectors $\mathbf{x}^M_{,\xi}$, $\mathbf{x}^L_{,\eta}$ and the matrices $\mathbf{T}_I, \hat{\mathbf{M}}_I(\mathbf{h}_I)$ are specified in Ref. [11].

Funding Open Access funding enabled and organized by Projekt DEAL.

References

1. MacNeal RH (1978) A simple quadrilateral shell element. Comput Struct 8:175–183
2. Hughes TJR, Tezduyar TE (1981) Finite elements based upon Mindlin plate theory, with particular reference to the 4-node bilinear isoparametric element. Appl Mech 48:587–595
3. MacNeal RH (1982) Derivation of element stiffness matrices by assumed strain distribution. Nucl Eng Design 70:3–12
4. Dvorkin E, Bathe K-J (1984) A continuum mechanics based four node shell element for general nonlinear analysis. Eng Comput 1:77–88
5. Choi CK, Paik JG (1994) An efficient four node degenerated shell element based on the assumed covariant strain. Struct Eng Mech 2(1):17–34
6. Koschnick F, Bischoff M, Camprubí N, Bletzinger K-U (2005) The discrete strain gap method and membrane locking. Comput Methods Appl Mech Eng 194:2444–2463
7. Kulikov GM, Plotnikova SV (2010) A family of ANS four-node exact geometry shell elements in general convected curvilinear coordinates. Int J Numer Methods Eng 83(10):1376–1406
8. Sze KY, Chow CL (1991) A mixed formulation of a 4-node Mindlin shell/plate with interpolated covariant transverse-shear strains. Comput Struct 40(3):775–784
9. Wiśniewski K, Turska E (2008) Improved four-node Hellinger-Reissner elements based on skew coordinates. Int J Numer Methods Eng 76:798–836
10. Kulikov GM, Plotnikova SV (2002) Efficient mixed Timoshenko-Mindlin shell elements. Int J Numer Methods Eng 55:1167–1183
11. Wagner W, Gruttmann F (2005) A robust nonlinear mixed hybrid quadrilateral shell element. Int J Numer Methods Eng 64:635–666
12. Gruttmann F, Wagner W (2006) Structural analysis of composite laminates using a mixed hybrid shell element. Comp Mech 37:479–497
13. Wagner W, Gruttmann F (2020) An improved quadrilateral shell element based on the Hu-Washizu functional. Adv Model and Simul in Eng Sci 7:28. https://doi.org/10.1186/s40323-020-00162-5
14. Wiśniewski K, Turska E (2009) Improved 4-node Hu-Washizu elements based on skew coordinates. Comput Struct 87:407–424
15. Wiśniewski K, Wagner W, Turska E, Gruttmann F (2010) Four-node Hu-Washizu elements based on skew coordinates and contravariant assumed strains. Comput Struct 88:1278–1284
16. Lavrenčič M, Brank B (2019) Hybrid-mixed shell finite elements and implicit dynamic schemes for shell post-buckling. In: Chróścielewski J, Eremeyev VA, Wiśniewski K (eds) Recent developments in the theory of shells. Springer, Cham, pp 383–412
17. Lavrenčič M, Brank B (2020) Hybrid-mixed shell quadrilateral that allows for large solution steps and is low-sensitive to mesh distortion. Comput Mech 65:177–192
18. Lavrenčič M, Brank B (2021) Hybrid-mixed low-order finite elements for geometrically exact shell models: overview and comparison. Arch Comput Meth Eng 28:3917–3951
19. Simo JC, Rifai MS (1990) A class of mixed assumed strain methods and the method of incompatible modes. Int J Numer Methods Eng 29:1595–1638
20. Simo JC, Armero F (1992) Geometrically non-linear enhanced strain mixed methods and the method of incompatible modes. Int J Numer Methods Eng 33:1413–1449
21. Belytschko T, Tsay C-S (1983) A stabilization procedure for the quadrilateral plate element with one-point quadrature. Int J Numer Methods Eng 19:405–419
22. Belytschko T, Lin JI, Tsay C-S (1984) Explicit algorithms for the nonlinear dynamics of shells. Comput Methods Appl Mech Eng 42:225–251
23. Liu KK, Law SE, Lam D, Belytschko T (1986) Resultant-stress degenerated shell element. Comput Methods Appl Mech Eng 55:261–300
24. Belytschko T, Wong BL, Chiang HY (1992) Advances in one-point quadrature shell elements. Comput Methods Appl Mech Eng 96:93–107
25. Belytschko T, Leviathan I (1994) Physical stabilization of the 4-node shell element with one point quadrature. Comput Methods Appl Mech Eng 113:321–350
26. Zhu Y, Zacharia T (1996) A new one-point quadrature, quadrilateral shell element with drilling degree of freedom. Comput Methods Appl Mech Eng 136:165–203
27. Zeng Q, Combescure A (1998) A new one-point quadrature, general non-linear quadrilateral shell element with physical stabilization. Int J Numer Methods Eng 42:1307–1338
28. Cardoso RPR, Yoon J-W, Grácio JJ, Barlat F, César de Sá JMA (2002) Development of a one point quadrature shell element for nonlinear applications with contact and anisotropy. Comput Methods Appl Mech Eng 191:5177–5206
29. Cardoso RPR, Yoon J-W (2005) One point quadrature shell element with through-thickness stretch. Comput Meth Appl Mech Eng 194:1161–1199
30. Cardoso RPR, Yoon J-W, Fontes Valente RA (2007) Enhanced one-point quadrature shell element for nonlinear applications. Int J Numer Methods Eng 69:627–663
31. Cardoso RPR, Yoon J-W (2007) One point quadrature shell elements: a study on convergence and patch tests. Comput Mech 40:871–883
32. Gruttmann F, Wagner W (2005) A linear quadrilateral shell element with fast stiffness computation. Comput Meth Appl Mech Eng 194:4279–4300

33. Ko Y, Lee PS, Bathe K-J (2017) A new MITC4+ shell element. Comput Struct 182:404–418
34. Ko Y, Lee PS, Bathe K-J (2017) The MITC4+ shell element in geometric nonlinear analysis. Comput Struct 185:1–14
35. Cui X, Peng G, Ran Q, Zhang H, Li S (2024) Derivation and implementation of one-point quadrature quadrilateral shell element with MITC4+ method (MITC4+R). Comput Struct 291:107207
36. Reese S, Wriggers P, Reddy BD (2000) A new locking-free brick element technique for large deformation problems in elasticity. Comput Struct 75:291–304
37. Reese S, Wriggers P (2000) A stabilization technique to avoid hourglassing in finite elasticity. Int J Numer Meth Eng 48:79–109
38. Reese S (2007) A large deformation solid-shell concept based on reduced integration with hourglass stabilization. Int J Numer Meth Eng 69:1671–1716
39. Schwarze M, Reese S (2011) A reduced integration solid-shell finite element based on the EAS and the ANS concept-Large deformation problems. Int J Numer Meth Eng 85:289–329
40. Gruttmann F, Wagner W (2024) A FE2 shell model with periodic boundary conditions for thin and thick shells. Int J Numer Meth Eng 125(11):e7433
41. Simo JC, Fox DD, Rifai MS (1990) On a stress resultant geometrically exact shell model. Part III: computational aspects of the nonlinear theory. Comput Meth Appl Mech Eng 79:21–70
42. Pian THH, Sumihara K (1984) Rational approach for assumed stress finite elements. Int J Numer Meth Eng 20(9):1685–1695
43. Gruttmann F, Wagner W (2020) An advanced shell model for the analysis of geometrical and material nonlinear shells. Comput Mech 66:1353–1376. https://doi.org/10.1007/s00466-020-01905-2
44. Magisano D, Leonetti L, Garcea G (2017) How to improve efficiency and robustness of the Newton method in geometrically non-linear structural problem discretized via displacement-based finite elements. Comput Meth Appl Mech Eng 313:986–1005
45. Pfefferkorn R, Bieber S, Oesterle B, Bischoff M, Betsch P (2020) Improving efficiency and robustness of enhanced assumed strain elements for nonlinear problems. Int J Numer Meth Eng 122(8):1911–1939
46. Taylor RL (2025) FEAP. http://www.ce.berkeley.edu/projects/feap/
47. MacNeal RH, Harder RL (1985) A proposed standard set of problems to test finite element accuracy. Finite Elem Anal Des 1:3-20
48. Wiśniewski K, Turska E (2012) Four-node mixed Hu-Washizu shell element with drilling rotation. Int J Numer Meth Eng 90:506–536
49. Knight NF (1997) Raasch challenge for shell elements. AIAA J 35(2):375–81
50. Chróścielewski J, Makowski J, Stumpf H (1992) Genuinely resultant shell finite elements accounting for geometric and material non-linearities. Int J Numer Meth Eng 35:63–94
51. Ibrahimbegović A, Frey F (1994) Stress resultant geometrically nonlinear shell theory with drilling rotation part II: computational aspects. Comput Meth Appl Mech Eng 188:285–308
52. Betsch P, Gruttmann F, Stein E (1996) A 4-node finite shell element for the implementation of general hyperelastic 3D-elasticity at finite strains. Comput Meth Appl Mech Eng 130:57–79
53. Eberlein R, Wriggers P (1999) Finite element concepts for finite elastoplastic strains and isotropic stress response in shells: theoretical and computational analysis. Comput Meth Appl Mech Eng 171:243–279
54. Fontes Valente RA, Parente MPL, Natal Jorge RM, César de Sá JMA, Gracio JJ (2005) Enhanced transverse shear strain shell formulation applied to elasto-plastic deformation problems. Int J Numer Meth Eng 62:1360–1398
55. Chróścielewski J, Witkowski W (2006) Four-node semi-EAS element in six-field nonlinear theory of shells. Int J Numer Meth Eng 68:1137–1179
56. Klinkel S, Gruttmann F, Wagner W (2008) A mixed shell formulation accounting for thickness strains and finite strain 3d material models. Int J Numer Meth Eng 74:945–970
57. Klinkel S, Gruttmann F, Wagner W (2006) A robust non-linear solid shell element based on a mixed variational formulation. Comput Meth Appl Mech Eng 195:179–201
58. Schürg M, Wagner W, Gruttmann F (2009) An enhanced FSDT model for the calculation of interlaminar shear stresses in composite plate structures. Comput Mech 44(6):765–776